Neoproterozoic granitoids from the Phan Si Pan belt, Northwest Vietnam: Implication for the tectonic linkage between Northwest Vietnam and the Yangtze Block

Xiao-Chun Li [a], Jun-Hong Zhao [b,*], Mei-Fu Zhou [a], Jian-Feng Gao [c], Wei-Hua Sun [d], MyDung Tran [e]

[a] Department of Earth Sciences, University of Hong Kong, Hong Kong Special Administrative Region
[b] State Key Laboratory of Geological Processes and Mineral Resources, China University of Geosciences, Wuhan 430074, China
[c] State Key Laboratory of Ore Deposit Geochemistry, Institute of Geochemistry, Chinese Academy of Sciences, Guiyang 550002, China
[d] School of Earth Sciences and Resources, China University of Geosciences, Beijing 100083, China
[e] General Department of Geology and Minerals of Vietnam, Vietnam

ARTICLE INFO

ABSTRACT

Several Neoproterozoic granitic intrusions, including the Phin Ngan intrusion and some smaller ones from the Sin Quyen Cu mine, have been identified in the Phan Si Pan belt, Northwest Vietnam. Whole-rock geochemical and Sm-Nd isotopic data and zircon U-Pb age and Hf-O isotopes have been determined for these intrusions in order to constrain their ages, petrogenesis and tectonic implications. The Phin Ngan intrusion, mainly composed of syenogranite, was emplaced at 824 ± 4 Ma. Rocks from this intrusion have high SiO_2 (72.1–73.5 wt.%), and K_2O (5.14–5.52 wt.%), with A/CNK values ranging from 1.02 to 1.06. They have negative whole-rock $\varepsilon_{Nd}(t)$ (−8.4 to −5.2) and zircon $\varepsilon_{Hf}(t)$ values (−8.1 to −5.5), and high zircon $\delta^{18}O$ values (9.7–10.9‰). These geochemical features suggest that the Phin Ngan intrusion was derived from ancient, K-rich crustal sources. Granitic intrusions from the Sin Quyen mine occur as stocks or dykes intruding ores and ore-hosting rocks. They are composed of monzogranite and granodiorite, emplaced between 736 ± 8 and 758 ± 6 Ma. They have high SiO_2 (68.2–76.7 wt.%) and $(K_2O + Na_2O)$ (6.93–8.54 wt.%), and low MgO (0.19–0.87), with A/CNK values ranging from 0.91 to 1.14. Their whole-rock $\varepsilon_{Nd}(t)$ values range from −6.6 to 0, mostly clustered between −6.6 and −4.3. Their zircon $\varepsilon_{Hf}(t)$ values vary from −6.7 to +11.1, mostly lower than −2.0. Such geochemical data indicate that these intrusions were produced mainly through partial melting of ancient crustal materials, coupled with subordinate involvement of mantle-/juvenile crust-derived components. The Phin Ngan intrusion and intrusions from the Sin Quyen mine are sub-alkaline in nature, and have arc-like trace-element compositions. Compiled with other broadly synchronous igneous rocks with arc-like affinities in the region, the Neoproterozoic magmatism in the Phan Si Pan belt was generated in a subduction-related setting. The Neoproterozoic intrusions in the Phan Si Pan belt are geochronologically and geochemically correlated with the Neoproterozoic subduction-related igneous rocks along the western Yangtze Block. Thus, the Phan Si Pan belt represents the southern most part of the giant arc system of the western Yangtze Block.

© 2017 Elsevier B.V. All rights reserved.

1. Introduction

The geology of Northwest Vietnam is characterized by two important tectonothermal events. One is the activation of the sinistral Ailao Shan-Red River (ASRR) shear zone resulted from the Cenozoic India-Asia collision. The activation of the ASRR shear zone led to a large-scale displacement of the Indochina peninsula relative to South China (Tapponnier et al., 1990; Fig. 1). The other event is the assembly of the Indochina and South China Blocks (Lepvrier et al., 2004). The Indochina Block is considered to have been derived from the northern margin of Gondwanaland and drifted northward in the Devonian (Metcalfe, 2002, 2006). By the Late Triassic, the Indochina block had amalgamated with the South China Block (Liu et al., 2015). Due to the diachronous episodes of metamorphism and deformation in the region, the geotectonic evolution of Northwest Vietnam is not well understood. One of the key questions is the tectonic attribution of Northwest Vietnam.

A number of mafic and ultramafic intrusions crop out in the middle segment of the Ailao Shan shear zone, South China (Fig. 2), which are regarded as remnants of obducted Tethyan ophiolites (Yumul Jr. et al., 2008). On this basis, the whole ASRR shear zone was viewed as
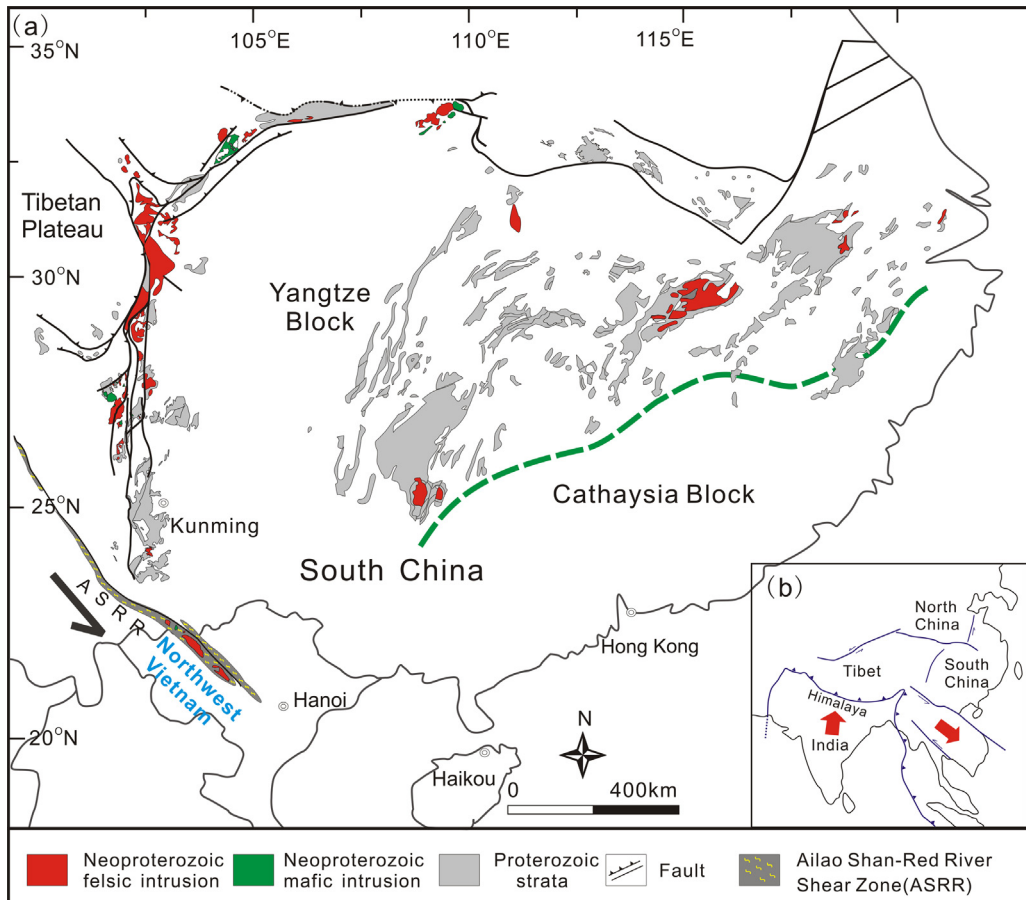
Fig. 1. (a) Simplified regional map highlighting the distribution of Neoproterozoic igneous rocks within the Yangtze Block, South China and Northwest Vietnam (after Zhao et al., 2011). (b) Major Cenozoic fault systems in Asia, illustrating continent excursion in response to India-Asia collision (after Tapponnier et al., 1990).

a suture belt, which separates the South China Block on the northeast from the Indochina Block on the southwest (e.g., Tapponnier et al., 1990; Leloup et al., 1995; Roger et al., 2000), i.e., Northwest Vietnam was thought to be part of the Indochina Block (Qi et al., 2012, 2014). Alternatively, the boundary between the South China and Indochina Blocks was inferred to lie along the more southerly Song Ma belt (e.g., Chung et al., 1997; Lepvrier et al., 1997; Faure et al., 2014; Fig. 2), where serpentinite slivers, MORB-like metabasaltic rocks, and eclogites are present. The southeastern part of the ASRR Shear Zone was therefore redefined as an intracontinental fault system, and Northwest Vietnam was regarded as a southeastward displaced part of the South China Block.

Granitoids are the major components of the continental crust, and thus bear important information about the crustal evolution and tectonic history (e.g., Chappell et al., 1987; Jahn et al., 2000). The Posen granitic pluton is recognized to have emplaced at ~760 Ma in the Phan Si Pan belt of Northwest Vietnam (Fig. 3; Wang et al., 2011). Recently, several smaller Neoproterozoic granitic intrusions have been identified in this belt, which have different ages from the Posen intrusion. The newly identified intrusions, together with the Posen pluton, might be geochronologically correlated with the widespread Neoproterozoic igneous rocks (~710 to ~870 Ma) along the margins of the Yangtze Block in South China (Zhao and Cawood, 2012 and references therein; Fig. 1). Thus, the Neoproterozoic intrusions from the Phan Si Pan belt provide a good opportunity to address the nature of the continental crust in Northwest Vietnam, and the possible tectonic linkage between Northwest Vietnam and the Yangtze Block in South China. In this study, we present whole-rock geochemical and Sm-Nd isotopic data and *in-situ* zircon U-Pb and Hf-O isotopes for the newly

identified Neoproterozoic granitoids in the Phan Si Pan belt, in order to decipher the petrogenesis and tectonic settings of the granitoids, and to discuss the tectonic attribution of Northwest Vietnam.

2. Geological background

Northwest Vietnam is bounded by the Red River fault to the north, and the Song Ma belt to the south (Fig. 2). Three major tectonic zones occur in Northwest Vietnam, namely the Phan Si Pan belt, Song Da rift and Tu Le Basin.

The Phan Si Pan belt is the southeastward continuation of the Ailao Shan belt in South China. The Phan Si Pan belt mainly contains a high-grade metamorphic complex that is composed mainly of biotite schist, two-mica schist, granitic gneiss, biotite-amphibole gneiss and graphite-bearing marble (Fig. 3), which are defined as the Suoi Chieng and Sin Quyen Groups. The protoliths of the metamorphic complex include Archean to Paleoproterozoic granitoids (e.g., ~2.8 Ga Cavinh complex, Lan et al., 2001; ~2.3 Ga Xom Giau granitic complex, Nam, 2001), and Paleoproterozoic to Neoproterozoic sediments and mafic volcanic rocks (e.g., Pham et al., 2010, 2012; Wang et al., 2016). This complex has been metamorphosed to greenschist to amphibolite facies during multiple geological events (e.g.,~1.8 Ga, ~250 Ma, and ~30 Ma) (Pham et al., 2012; Wang et al., 2016). The metamorphic complex is unconformably covered by Paleozoic-Early Triassic sedimentary rocks. A number of Neoproterozoic granitoids intrude the metamorphic complex, among which the 760 Ma Posen intrusion is the largest one (Fig. 3). Previous studies suggest that the Posen intrusion was produced through reworking of Paleoproterozoic crust by
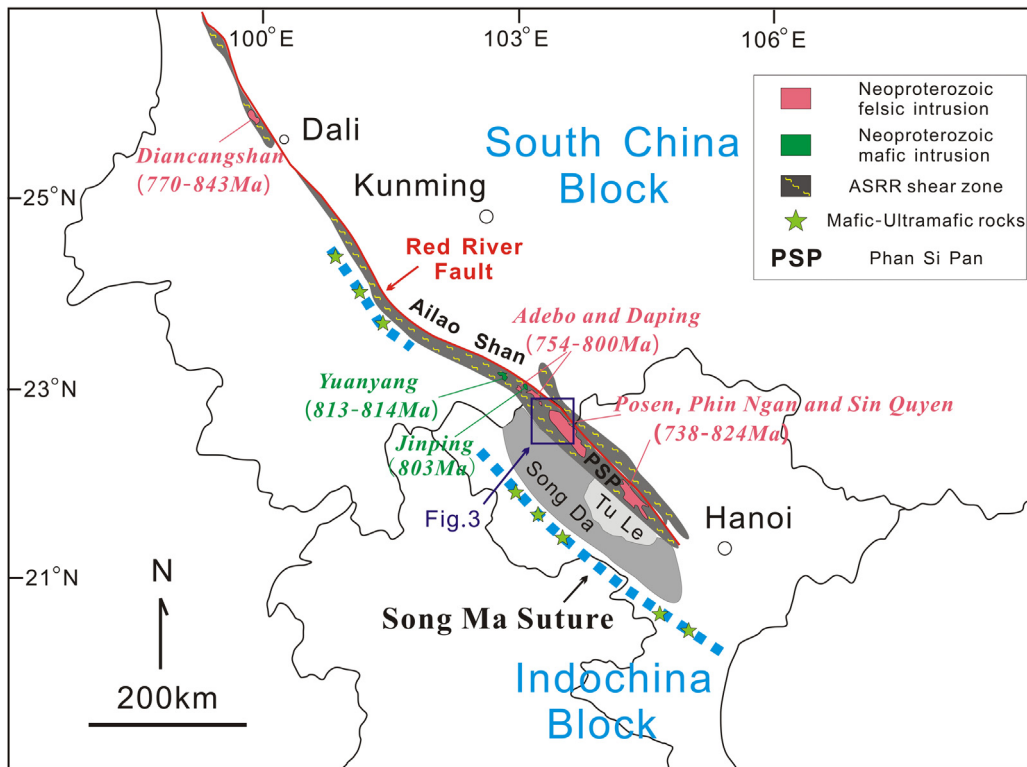
Fig. 2. Simplified geotectonic map of northwestern Vietnam and southwestern China, showing the location of major tectonic units and highlighting the distribution of Neoproterozoic igneous rocks. The ages of the Diancangshan felsic intrusions are from Liu et al. (2008a) and Lin et al., (2012); Yuanyang and Jinping mafic intrusions from Cai et al. (2014); Adebo and Daping felsic intrusions from Qi et al., (2012) and Cai et al., (2015); Posen intrusion, Phin Ngan intrusion and intrusions in the Sin Quyen mine from Wang et al., (2011) and this study.

mantle-derived magmas (Lan et al., 2000; Pham et al., 2009). Some late Permian to early Triassic (249–259 Ma) alkaline to sub-alkaline felsic intrusions occur in southwest portion of the Phan Si Pan belt (Fig. 3), which are though to be genetically related to mantle plume activity (Usuki et al., 2015). Several Fe-Cu mines or prospects are distributed along the Phan Si Pan belt, including Sin Quyen, Nam Mit, Nam Chac, Suoi Thau, and Lung Thang (McLean, 2001). Among them, the Sin Quyen Cu-LREE-Au deposit is the largest one, and it is currently the largest Cu producer in Vietnam (Figs. 3 and 4).

The Song Da rift mainly contains Devonian to Middle Triassic sedimentary-volcanic sequences, which are unconformably overlain by Late Triassic conglomerates and sandstones or by Cretaceous continental red beds. It is notable that a Late Permian (∼260 Ma) ultramafic-mafic volcanic suite, mainly picrites and flood basalts, are well developed in the Song Da rift, particularly along the Da River (Polyakov et al., 1998). The volcanic rock suite rests on early Permian limestone and is unconformably overlain by Triassic limestone and shale with coal seams (Tran et al., 2011; Metcalfe, 2012). An acidic to intermediate magmatic suite, known as the "Tu Le volcanic rocks", is developed in the Tu Le basin. The Tu Le volcanic rocks are mainly composed of rhyolite, trachyrhyolite and trachydacite. Recent studies revealed that the felsic rock suite (249–262 Ma) in the Tu Le basin is coeval with the mafic rock suite in the Song Da rift (Tran et al., 2015; Usuki et al., 2015).

3. Sample description

3.1. Phin Ngan intrusion

The Phin Ngan intrusion is located to the northwest of the Phin Ngan town, and covers an area of ∼5 km² (Fig. 3). It intrudes the meta-sedimentary rocks of the Sin Quyen Group. This intrusion

generally shows NW-SE trending schistosity (Fig. 5a). The Phin Ngan intrusion is composed of syenogranite, which is medium- to coarse-grained, and consists mainly of alkaline feldspar (30–45%), plagioclase (15–20%), quartz (20–25%) and biotite (8%) (Fig. 5b). The accessory minerals in this intrusion include titanite, opaque oxides, zircon and apatite. Subhedral to anhedral alkaline feldspar is medium- to coarse-grained (with length of 100–300 μm), and usually shows simple twining and/or perthitic textures. Many alkaline feldspar crystals have embayed margins, and locally enclose plagioclase and quartz. Subhedral plagioclase is relatively small (with length of 30–100 μm), and shows well-developed polysynthetic twinning and/or concentric zoning. Locally, plagioclase is altered to sericite and epidote. Biotite commonly occurs as aggregates defining the schistosity, and was locally replaced by chlorite. Quartz commonly forms recrystallized sub-grains in response to deformation.

3.2. Intrusions from the Sin Quyen mining district

Numerous granitic stocks or dykes intrude Proterozoic metasedimentary rocks or Cu ores in the Sin Quyen mining district (Figs. 4, 5c and 5d). They show different sizes (5–200 m by 2–100 m) and shapes, and have undergone variable deformation. These intrusions are composed of monzogranite and granodiorite. They are medium-grained, and consist mainly of alkaline feldspar (10–35%), plagioclase (25–55%), quartz (20–25%), and biotite (5–8%) (Figs. 5e and f). Some samples (SQ15-09 and SQ-80A) also contain minor amounts of hornblende (5–10%) (Figs. 5f and g). The accessory minerals include oxides, zircon, titanite and apatite. Alkaline feldspar forms subhedral to anhedral grains with length of 50–200 μm, and usually shows simple twining, cross-hatched twinning and/or perthitic textures. The relatively large alkaline feldspar grains show resorbed edges, and enclose some biotite, plagioclase,
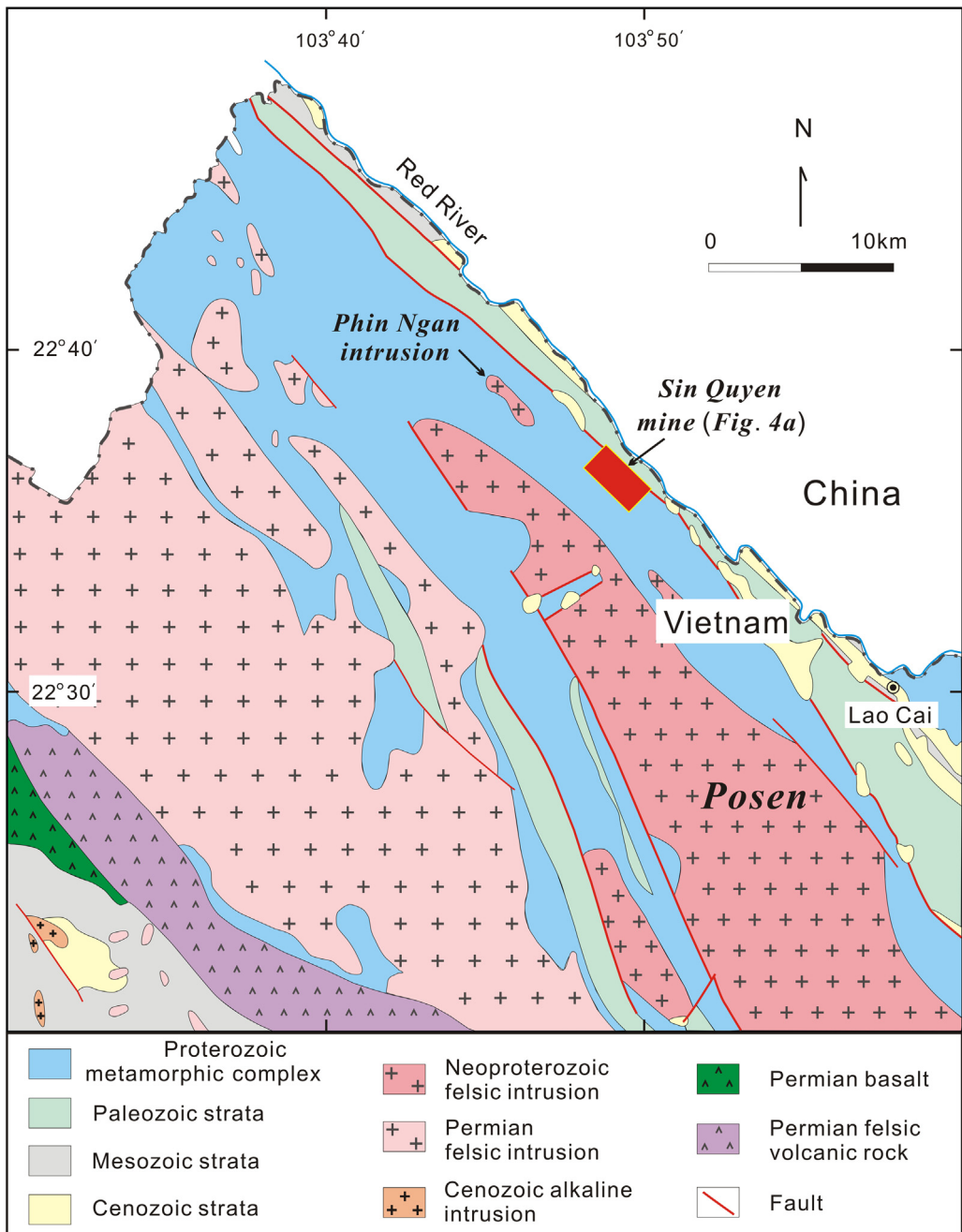
Fig. 3. Geological map of the Sin Quyen area in the Phan Si Pan belt (modified after 1:200,000 geological map).

and quartz. Plagioclase occurs as either single grains (Figs. 5e and f), with variable sizes (with length of 50–250 μm), or massive aggregates up to 1 cm in length (Fig. 5h). It shows well-developed polysynthetic twinning, concentric zoning and/or clean margin texture. Locally, plagioclase is altered to sericite and/or epidote. Biotite and hornblende form disseminated, euhedral to subhedral grains of 100–200 μm in length. Biotite usually shows directional arrangement, and may be partially altered to muscovite or chlorite. Quartz is commonly interstitial to feldspar and biotite.

4. Analytical methods

4.1. LA-ICP-MS zircon U-Pb dating

Prior to U-Pb isotopic analyses, zircon was examined with transmitted and reflected light and further with cathodoluminescence

(CL) images to reveal their internal textures. Zircon U-Pb dating was conducted by laser ablation-inductively coupled plasma-mass spectrometry (LA-ICP-MS) at the State Key Laboratory of Geological Processes and Mineral Resources, China University of Geosciences, Wuhan. Detailed operating conditions are similar as described by Liu et al. (2008b). Laser sampling was performed using a GeoLas 2005. An Agilent 7500a ICP-MS instrument was used to acquire ion-signal intensities. Helium was applied as a carrier gas. Argon was used as the make-up gas and mixed with the carrier gas via a T-connector before entering the ICP. Nitrogen was added into the central gas flow (Ar + He) of the Ar plasma to decrease the detection limit and improve precision. Analyses were performed with a beam diameter of 44 um and a repetition rate of 6 Hz. Each analysis incorporated a background acquisition of ~20 s followed by ~50 s data acquisition for the sample. Zircon 91500 was used as external standard for U-Pb dating.
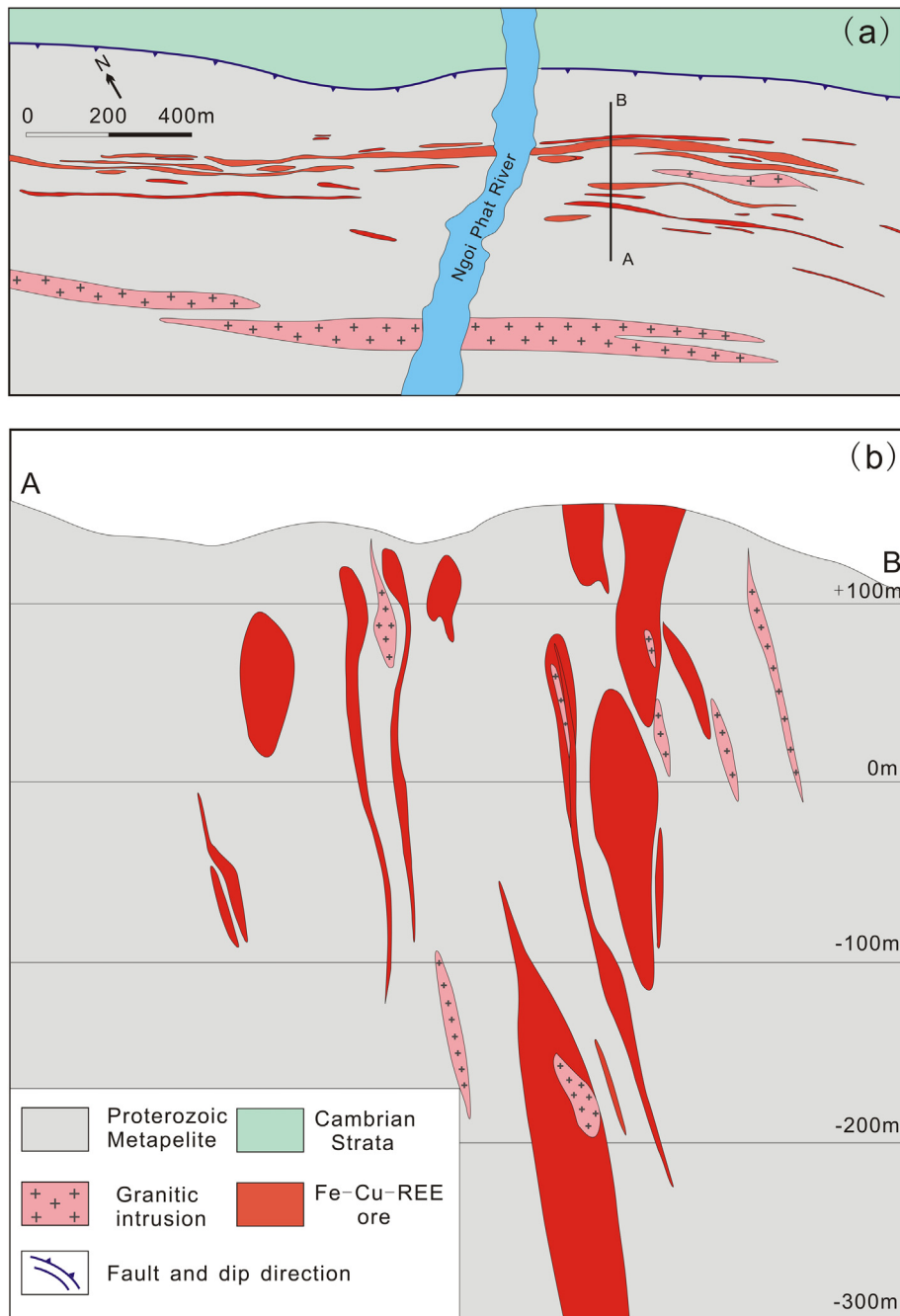
Fig. 4. (a) Simplified geological map of the Sin Quyen mine. (b) Cross section A-B located in (a), showing the shape and distribution of orebodies and granitic intrusions (after McLean, 2001).

Time-dependent drifts of U-Th-Pb isotopic ratios were corrected using a linear interpolation (with time) for every eight analyses according to the variations of 91500 (i.e., two 91500 standards + eight samples + two 91500 standards). U-Th-Pb isotopic ratios for 91500 are from Wiedenbeck et al. (1995). Uncertainty of preferred values for the external standard 91500 was propagated to the ultimate results of the samples. Off-line selection and integration of signals, and time-drift correction and quantitative calibration for trace element analyses and U-Pb dating were performed by *ICPMSDataCal* (Liu et al., 2008b). Concordia diagrams and weighted mean age calculations were made using Isoplot/Ex_ver3. In order to monitor the external uncertainties of measurements, a zircon standard GJ-1 was analyzed. Five measurements yielded a weighted

average $^{206}Pb/^{238}U$ age of 606 ± 4 Ma, which is in agreement with the recommended age of 608.5 ± 0.4 Ma (Jackson et al., 2004).

4.2. Whole-rock major and trace element analysis

Major element contents of bulk rocks were obtained at The University of Hong Kong. Mixtures of whole-rock powder (0.5 g) and $Li_2B_4O_7$ + $LiBO_2$ (5 g) were heated and fused into glass disks. The glass was analyzed by X-ray fluorescence spectroscopy (XRF) with an AXIOS Minerals spectrometer. Precisions are ±1–3% relative for elements in concentrations of >1 wt.%, and about ±10% relative for elements in concentrations of <1 wt.%. Trace elements were analyzed by Quadrupole ICP-MS at the State Key Laboratory
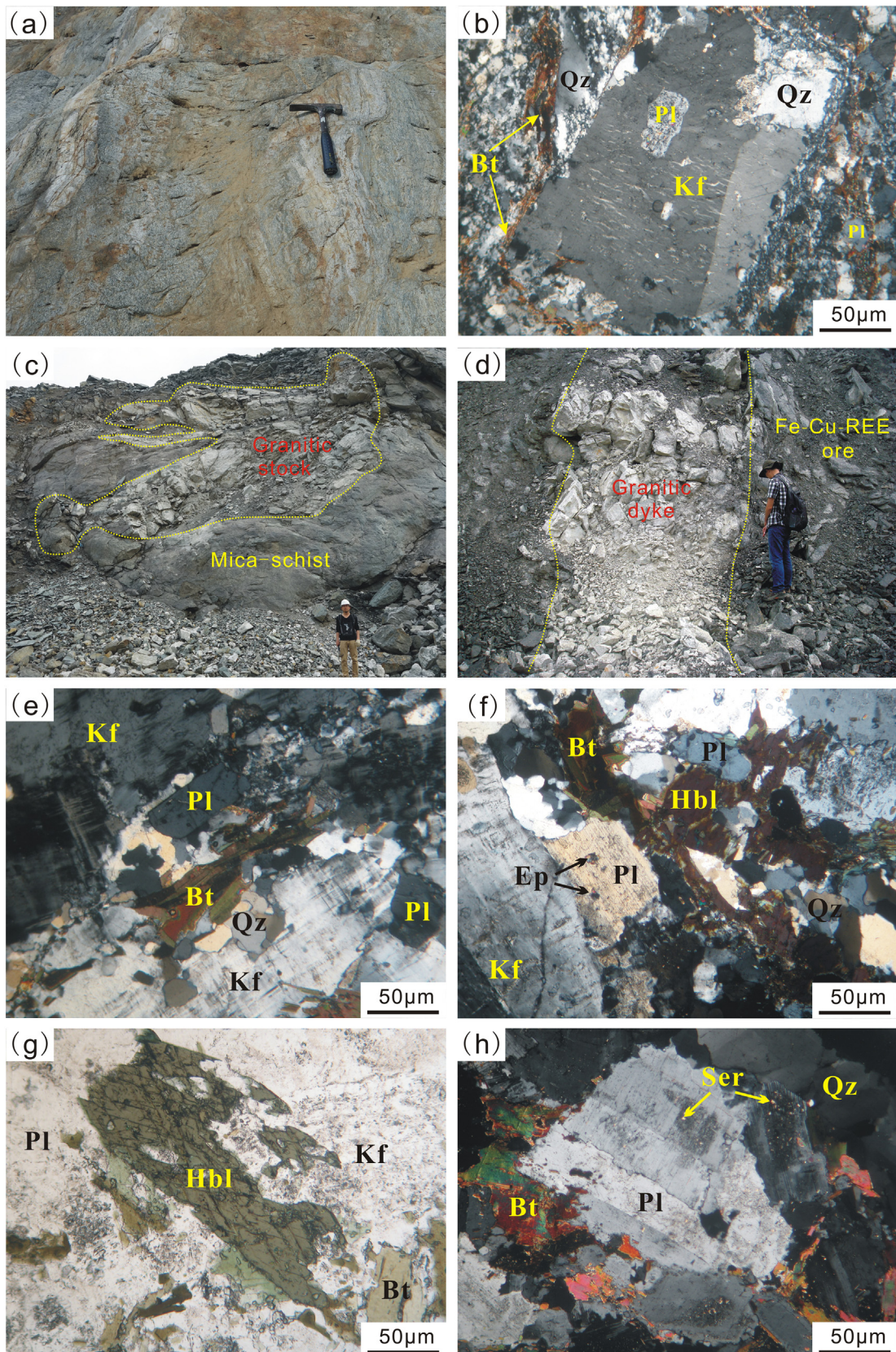
Fig. 5. (a) Field photo of the Phin Ngan intrusion, which shows schistosity along the NW direction. (b) The Phin Ngan intrusion consists of K-feldspar, plagioclase, quartz, and biotite. K-feldspar occurs as phenocryst, and contains plagioclase inclusions. (c) Field photo of a granitic stock in the Sin Quyen mine. (d) Field photo of a granitic dyke in the Sin Quyen mine. (e) An intrusion from the Sin Quyen mine shows typical granitic texture, and mainly consists of K-feldspar, plagioclase, quartz, and biotite. (f) One intrusion is mainly consists of K-feldspar, plagioclase, quartz, hornblende and biotite. Note that plagioclase is partially altered to epidote. (g) Hornblende in an intrusion from the Sin Quyen mine. (h) Plagioclase aggregate in one intrusion from the Sin Quyen mine. Some portions of the plagioclase have been replaced by sericite. Abbreviations: Bt: biotite, Ep: epidote, Hbl: hornblende, Kf: K-feldspar, Pl: plagioclase, Qz: quartz, Ser: sericite.

of Ore Deposit Geochemistry, Institute of Geochemistry, Chinese Academy of Sciences, Guiyang. Detailed procedures have been described by Qi et al. (2000). The whole rock powders were dissolved by distilled HNO_3 and HF. Closed beakers in high-pressure bombs were used to ensure complete digestion. Dissolved samples were diluted to 49 ml with 1% HNO_3, and 1 ml 500 ppb indium was added to the solution as an internal standard. The analytical precisions are generally better than 5% for most elements based on replicate analyses of standard samples.

4.3. Whole-rock Sm-Nd isotopic analysis

The Sm-Nd isotopic compositions were analyzed at Institute of Geochemistry, Chinese Academy of Sciences. About 100 mg sample powder was dissolved by HF + HNO_3 + $HClO_4$. Chemical separation was performed using two-stage ion exchange procedures similar to the methods described by Chen et al. (2002). Firstly, REE were isolated from the matrix elements using a standard cation exchange resin. After that, Sm and Nd were separated using Eichrom LN (LN-C-50B, 100–150 μm, 2 ml) chromatographic columns. The Nd isotopic ratios were measured using a Thermo Scientific Neptune Multicollector (MC)-ICP-MS. The measured Nd isotopic ratios were normalized to $^{146}Nd/^{144}Nd = 0.7219$. During the period of data collection, the average measured value for the JNdi-1 Nd standard was $^{143}Nd/^{144}Nd = 0.512102$. The rock standard BCR-2 was measured to monitor the accuracy of the analytical procedure, and a $^{143}Nd/^{144}Nd$ ratio of 0.512671 ± 15 (2σ) was obtained, which is comparable with the reported reference values (GeoREM, http://georem.mpch-mainz.gwdg.de/). The $^{147}Sm/^{144}Nd$ ratios were calculated from the concentrations of Sm and Nd measured by ICP-MS. The adopted decay constant for ^{147}Sm is 6.54×10^{-12} year^{-1} (Lugmair and Harti, 1978). The $\varepsilon_{Nd}(t)$ values were calculated according to the chondritic values of Lugmair and Harti (1978).

4.4. Zircon Lu-Hf isotopic analysis

In-situ zircon Lu-Hf isotopic analyses were conducted using a New Wave ArF 193 nm laser ablation system attached to a Neptune MC–ICP-MS (plus) at Nanjing University. The detailed analytical procedure and correction for interferences followed that described by Wu et al. (2006). Both He and Ar carrier gases were used to transport the ablated sample from the laser-ablation cell via a mixing chamber to the ICP–MS torch. Laser spot size of 32 μm and repetition rate of 8 Hz with energy density of 12 J/cm^2 were used during the analyses. Raw count rates for ^{172}Yb, ^{173}Yb, ^{175}Lu, ^{176}(Hf + Yb + Lu), ^{177}Hf, ^{178}Hf, ^{179}Hf, ^{180}Hf and ^{182}W were collected. Isobaric interference corrections for ^{176}Lu and ^{176}Yb on ^{176}Hf must be determined precisely. ^{176}Lu was calibrated using the ^{175}Lu value. The $^{176}Yb/^{172}Yb$ value of 0.5887 and mean β_{Yb} value obtained during Hf analysis on the same spot were applied for the interference correction of ^{176}Yb on ^{176}Hf. During analyses, the $^{176}Hf/^{177}Hf$ ratios of the standards zircon 91500 and Mud Tank were 0.282312 ± 25 (2SE, n = 7) and 0.282496 ± 18 (2SE, n = 13), respectively, consistent within errors with the recommended ratios of 0.282302 ± 8 (Goolaerts et al., 2004) and 0.282523 ± 8 (Griffin et al., 2006), respectively. The adopted decay constant for ^{176}Lu is 1.867×10^{-11} year^{-1} (Söderlund et al., 2004). The $\varepsilon_{Hf}(t)$ values were calculated according to the chondrite values of Bouvier et al. (2008).

4.5. Zircon O isotopic analysis

Oxygen isotopic composition of zircon was measured using the CAMECA IMS-1280 SIMS at Institute of Geology and Geophysics, Chinese Academy of Sciences. The detailed analytical procedures were described by Li et al. (2010). The Cs$^+$ primary ion beam was accelerated at 10 kV, with an intensity of 2 nA corresponding to a
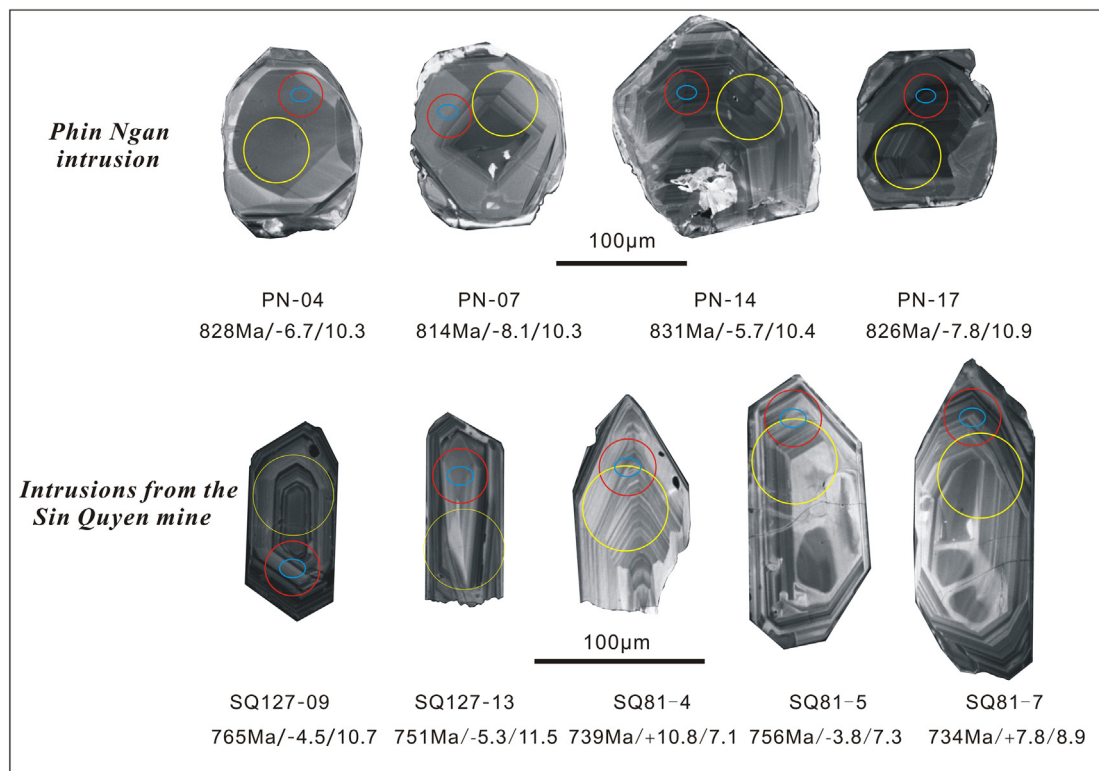
Fig. 6. Representative cathodoluminescent (CL) images of zircon grains. Red circles show the location of LA-ICP-MS U-Pb analyses; yellow circles show the location of the LA-MC-ICP-MS Hf isotope analyses; blue ellipses show the location of SIMS O isotope analyses. The analytical results are shown in the form of "age/$\varepsilon_{Hf}(t)$/δ^{18}O". (For interpretation of the references to color in this figure legend, the reader is referred to the web version of this article.)

Table 1
LA-ICP-MS U–Pb data for zircon from the Phin Ngan intrusion and intrusions from the Sin Quyen mine.

	Th(ppm)	U(ppm)	^{207}Pb/^{206}Pb	±σ	^{207}Pb/^{235}U	±σ	^{206}Pb/^{238}U	±σ	^{207}Pb/^{206}Pb age(Ma)	±σ	^{207}Pb/^{235}U age(Ma)	±σ	^{206}Pb/^{238}U age (Ma)	±σ	Concordance
Phin Ngan intrusion															
PN-01	1103	527	0.0669	0.0015	1.278	0.030	0.1377	0.0010	835	46	836	13	832	6	99%
PN-02	1087	615	0.0654	0.0015	1.078	0.029	0.1186	0.0016	787	47	742	14	723	9	97%
PN-03	439	250	0.0660	0.0019	1.241	0.036	0.1360	0.0012	807	59	819	16	822	7	99%
PN-04	518	344	0.0663	0.0014	1.259	0.028	0.1370	0.0011	817	44	828	13	828	6	99%
PN-05	255	198	0.0654	0.0018	1.257	0.036	0.1390	0.0013	787	64	827	16	839	7	98%
PN-06	579	379	0.0652	0.0015	1.237	0.030	0.1372	0.0012	789	50	817	14	829	7	98%
PN-07	557	317	0.0654	0.0017	1.216	0.031	0.1346	0.0011	787	54	808	14	814	6	99%
PN-08	823	436	0.0659	0.0016	1.230	0.029	0.1352	0.0012	801	51	814	13	817	7	99%
PN-09	1570	638	0.0663	0.0014	1.269	0.028	0.1382	0.0012	817	43	832	13	834	7	99%
PN-10	433	205	0.0667	0.0019	1.274	0.038	0.1380	0.0013	828	59	834	17	833	7	99%
PN-11	435	310	0.0660	0.0016	1.227	0.029	0.1345	0.0012	807	45	813	13	814	7	99%
PN-12	675	347	0.0668	0.0015	1.275	0.029	0.1379	0.0010	831	46	835	13	833	6	99%
PN-13	649	445	0.0656	0.0013	1.226	0.026	0.1348	0.0011	794	43	812	12	815	6	99%
PN-14	430	300	0.0650	0.0017	1.240	0.032	0.1375	0.0012	776	54	819	15	831	7	98%
PN-15	630	285	0.0658	0.0017	1.240	0.032	0.1361	0.0011	798	54	819	14	823	7	99%
PN-16	556	455	0.0666	0.0016	1.261	0.030	0.1366	0.0012	833	50	828	14	825	7	99%
PN-17	1190	505	0.0658	0.0015	1.245	0.027	0.1366	0.0012	798	51	821	12	826	7	99%
PN-18	391	211	0.0682	0.0019	1.282	0.036	0.1356	0.0013	876	57	838	16	820	7	97%
PN-19	380	279	0.0666	0.0017	1.271	0.032	0.1378	0.0012	828	54	833	14	832	7	99%
PN-20	1421	593	0.0657	0.0013	1.227	0.025	0.1343	0.0010	798	36	813	11	812	6	99%
PN-21	842	349	0.0658	0.0014	1.234	0.026	0.1355	0.0011	798	44	816	12	819	6	99%
PN-22	1216	528	0.0647	0.0015	1.199	0.027	0.1338	0.0011	765	49	800	12	809	6	98%
PN-23	514	393	0.0677	0.0017	1.168	0.028	0.1243	0.0009	861	50	786	13	755	5	96%
Intrusions from the Sin Quyen mine															
SQ81-01	278	473	0.0618	0.0013	1.065	0.024	0.1234	0.0013	665	44	736	12	750	7	98%
SQ81-02	264	616	0.0606	0.0012	1.031	0.021	0.1216	0.0012	628	75	719	11	740	7	97%
SQ81-03	172	685	0.0607	0.0011	1.003	0.019	0.1179	0.0010	628	73	705	10	719	6	98%
SQ81-04	113	241	0.0624	0.0014	1.057	0.023	0.1215	0.0012	687	55	732	12	739	7	99%
SQ81-05	86	117	0.0674	0.0021	1.152	0.034	0.1244	0.0017	850	69	778	16	756	10	97%
SQ81-06	235	489	0.0635	0.0017	1.005	0.026	0.1129	0.0014	724	59	707	13	690	8	97%
SQ81-07	61	302	0.0627	0.0014	1.059	0.023	0.1205	0.0014	698	48	733	12	734	8	99%
SQ81-08	97	514	0.0654	0.0015	1.090	0.023	0.1188	0.0013	787	48	748	11	724	8	96%
SQ81-09	273	376	0.0647	0.0015	1.095	0.024	0.1208	0.0014	765	45	751	12	735	8	98%
SQ81-10	80	400	0.0651	0.0017	1.143	0.029	0.1253	0.0019	789	57	774	14	761	11	98%
SQ81-11	97	489	0.0629	0.0013	1.029	0.021	0.1165	0.0012	706	44	718	10	710	7	98%
SQ81-12	86	169	0.0649	0.0018	1.089	0.029	0.1209	0.0014	772	53	748	14	736	8	98%
SQ81-13	143	376	0.0653	0.0015	1.144	0.025	0.1250	0.0014	783	46	774	12	759	8	98%
SQ81-14	99	371	0.0637	0.0016	1.100	0.027	0.1234	0.0014	731	52	753	13	750	8	99%
SQ81-15	336	514	0.0619	0.0014	1.061	0.021	0.1231	0.0013	672	42	734	10	748	7	98%
SQ81-16	364	526	0.0637	0.0013	1.090	0.021	0.1225	0.0011	731	43	749	10	745	7	99%
SQ81-17	260	541	0.0621	0.0014	1.075	0.031	0.1232	0.0023	677	48	741	15	749	13	98%
SQ81-18	243	634	0.0610	0.0011	1.040	0.019	0.1219	0.0012	639	39	724	9	741	7	97%
SQ81-19	503	609	0.0616	0.0013	1.026	0.022	0.1188	0.0013	661	46	717	11	723	7	99%
SQ81-20	181	432	0.0634	0.0015	1.082	0.025	0.1223	0.0013	720	19	744	12	744	8	99%
SQ-94-1	418	755	0.0666	0.0021	1.131	0.035	0.1218	0.0013	833	67	768	17	741	7	96%
SQ-94-2	19	39	0.0886	0.0053	1.817	0.122	0.1471	0.0048	1394	115	1052	44	885	27	82%
SQ-94-3	222	442	0.0655	0.0020	1.113	0.034	0.1214	0.0013	791	63	759	16	739	7	97%
SQ-94-4	216	509	0.0664	0.0020	1.136	0.034	0.1226	0.0013	817	63	770	16	746	8	96%
SQ-94-5	152	276	0.0625	0.0025	1.065	0.041	0.1223	0.0014	692	84	736	20	744	8	99%
SQ-94-6	223	322	0.0698	0.0026	1.239	0.047	0.1271	0.0018	924	77	819	21	771	10	94%
SQ-94-7	126	273	0.0642	0.0023	1.087	0.037	0.1216	0.0014	748	74	747	18	740	8	99%
SQ-94-8	106	153	0.0628	0.0025	1.068	0.042	0.1222	0.0015	702	86	738	21	743	9	99%
SQ-94-9	100	153	0.0622	0.0025	1.052	0.042	0.1218	0.0014	683	87	730	21	741	8	98%
SQ-94-10	78	125	0.0672	0.0027	1.161	0.048	0.1239	0.0017	856	83	782	22	753	10	96%
SQ-94-11	206	407	0.0631	0.0019	1.075	0.032	0.1227	0.0013	722	63	741	16	746	8	99%
SQ-94-12	208	367	0.0642	0.0017	1.073	0.028	0.1208	0.0013	750	53	740	14	735	8	99%
SQ-94-13	60	77	0.0638	0.0035	1.012	0.052	0.1163	0.0017	744	116	710	26	709	10	99%
SQ-94-14	345	564	0.0631	0.0015	1.063	0.027	0.1219	0.0015	709	51	735	13	741	9	99%
SQ-94-15	87	150	0.0617	0.0021	1.043	0.037	0.1227	0.0017	665	74	725	18	746	10	97%
SQ-94-16	123	221	0.0628	0.0019	1.046	0.032	0.1209	0.0016	702	63	727	16	736	9	98%
SQ-94-17	156	916	0.0644	0.0013	1.078	0.024	0.1212	0.0012	754	44	743	12	737	7	99%
SQ-94-18	83	152	0.0623	0.0028	1.061	0.048	0.1232	0.0016	683	96	734	24	749	9	98%
SQ-94-19	169	284	0.0622	0.0017	1.039	0.028	0.1213	0.0013	681	59	723	14	738	7	97%
SQ-94-20	169	297	0.0631	0.0018	1.073	0.032	0.1228	0.0014	722	61	740	16	747	8	99%
SQ-94-21	91	205	0.0648	0.0024	1.084	0.043	0.1206	0.0016	769	78	746	21	734	9	98%
SQ-127-01	150	272	0.0637	0.0018	1.088	0.031	0.1237	0.0012	731	29	747	15	752	7	99%
SQ-127-02	106	150	0.0641	0.0022	1.099	0.039	0.1242	0.0012	744	42	753	19	755	7	99%
SQ-127-03	94	156	0.0651	0.0021	1.108	0.036	0.1236	0.0011	777	75	757	18	752	6	99%
SQ-127-04	148	167	0.0647	0.0020	1.106	0.035	0.1238	0.0012	765	66	756	17	752	7	99%
SQ-127-05	83	152	0.0654	0.0020	1.125	0.035	0.1248	0.0012	787	65	765	17	758	7	99%
SQ-127-06	152	449	0.0634	0.0015	1.126	0.028	0.1286	0.0011	720	19	766	13	780	6	98%

Table 1 (*continued*)

	Th(ppm)	U(ppm)	$^{207}Pb/^{206}Pb$	±σ	$^{207}Pb/^{235}U$	±σ	$^{206}Pb/^{238}U$	±σ	$^{207}Pb/^{206}Pb$ age(Ma)	±σ	$^{207}Pb/^{235}U$ age(Ma)	±σ	$^{206}Pb/^{238}U$ age (Ma)	±σ	Concordance
SQ-127-07	288	742	0.0639	0.0014	1.105	0.025	0.1252	0.0010	739	42	756	12	761	6	99%
SQ-127-08	360	861	0.0623	0.0014	1.057	0.026	0.1227	0.0012	683	55	732	13	746	7	98%
SQ-127-09	136	380	0.0612	0.0017	1.063	0.029	0.1260	0.0011	656	59	735	14	765	6	96%
SQ-127-10	145	870	0.0631	0.0013	1.036	0.023	0.1187	0.0011	722	51	722	12	723	6	99%
SQ-127-11	223	369	0.0641	0.0016	1.124	0.028	0.1270	0.0010	746	48	765	13	771	5	99%
SQ-127-12	103	226	0.0651	0.0017	1.151	0.031	0.1279	0.0011	789	57	778	15	776	6	99%
SQ-127-13	299	1105	0.0632	0.0012	1.084	0.020	0.1235	0.0008	717	45	745	10	751	5	99%
SQ-127-14	248	411	0.0636	0.0014	1.105	0.024	0.1253	0.0009	728	46	756	12	761	5	99%
SQ-127-15	251	320	0.0606	0.0017	1.049	0.028	0.1246	0.0011	633	62	728	14	757	6	96%
SQ-127-16	43	77	0.0649	0.0033	1.073	0.052	0.1217	0.0014	772	106	740	25	740	8	99%
SQ-127-17	117	216	0.0646	0.0020	1.138	0.036	0.1264	0.0012	761	67	771	17	767	7	99%
SQ-127-18	56	71	0.0642	0.0031	1.097	0.054	0.1234	0.0015	750	104	752	26	750	8	99%
SQ-127-19	183	324	0.0644	0.0016	1.125	0.027	0.1258	0.0010	754	53	765	13	764	6	99%
SQ-127-20	76	144	0.0599	0.0019	1.030	0.032	0.1244	0.0011	598	103	719	16	756	6	95%
SQ-127-21	201	276	0.0630	0.0016	1.109	0.028	0.1264	0.0010	709	52	758	13	767	6	98%
SQ-127-22	188	261	0.0639	0.0016	1.079	0.027	0.1218	0.0011	739	54	743	13	741	6	99%
SQ-127-23	74	157	0.0636	0.0021	1.112	0.036	0.1254	0.0012	728	69	759	18	761	7	99%
SQ-127-24	104	179	0.0634	0.0021	1.083	0.035	0.1231	0.0011	724	72	745	17	749	6	99%
SQ-127-25	199	269	0.0593	0.0020	0.980	0.031	0.1192	0.0012	589	72	694	16	726	7	95%
SQ-127-26	167	364	0.0644	0.0015	1.145	0.028	0.1276	0.0012	755	50	775	13	774	7	99%
SQ-127-27	99	173	0.0653	0.0022	1.093	0.035	0.1212	0.0012	783	66	750	17	737	7	98%

beam size of 10 μm in diameter. A normal incidence electron flood gun was used to compensate for sample charging. Negative secondary ions were extracted with a −10 kV potential. Oxygen isotopes were measured using multi-collection mode. Measured $^{18}O/^{16}O$ ratios were standardized to Vienna Standard Mean Ocean Water compositions (VSMOW, $^{18}O/^{16}O$ = 0.0020052), and then cor-

rected for the instrumental mass fractionation factor (IMF). The IMF was obtained using the Durango fluorapatite as a reference with a $\delta^{18}O$ value of 9.4‰ (Trotter et al., 2008). The internal precision of a single analysis is generally better than 0.2‰ (2σ standard error) for $^{18}O/^{16}O$ ratio. The Qinghu zircon standard was measured to monitor the accuracy of the analytical procedure. Fourteen
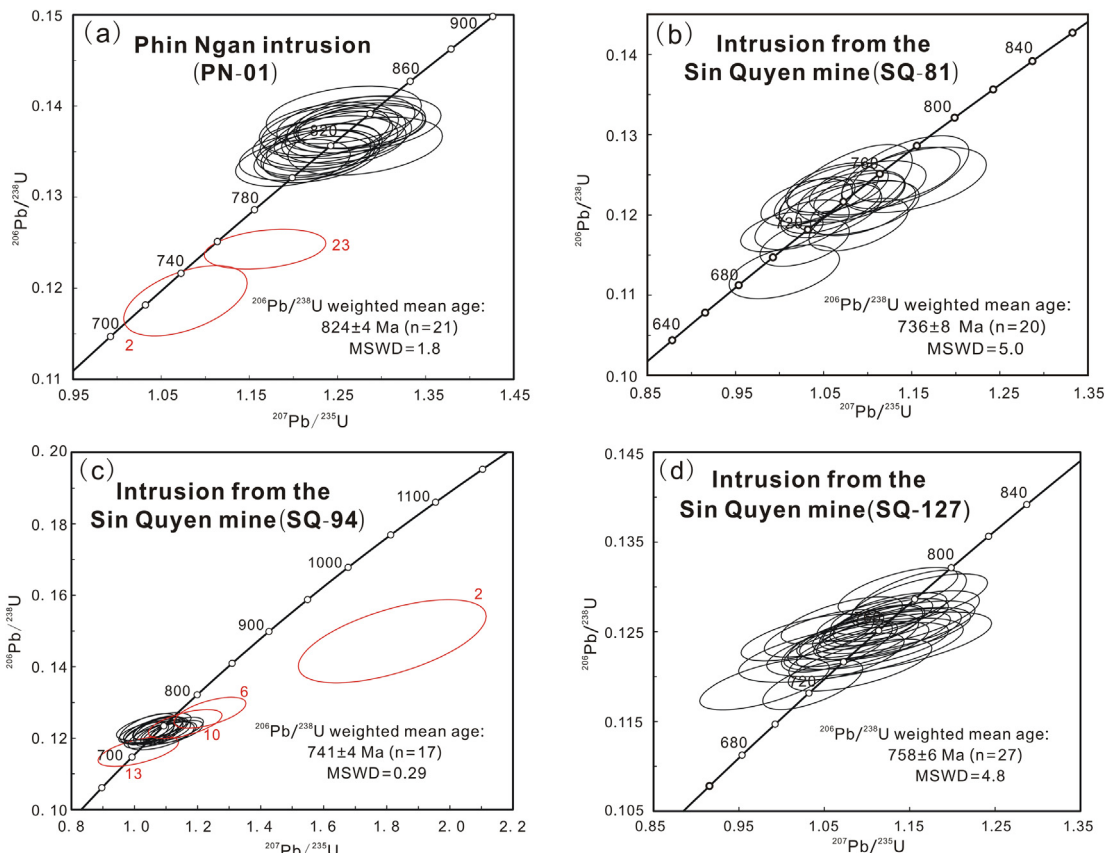

Fig. 7. Zircon U-Pb concordia diagrams for (a) the Phin Ngan intrusion, (b), (c) and (d) the intrusions from the Sin Quyen mine. Small numbers near red ellipses indicate analysis number mentioned in the text. (For interpretation of the references to color in this figure legend, the reader is referred to the web version of this article.)

measurements of the Qinghu zircon standard yielded a weighted mean δ¹⁸O value of 5.50 ± 0.11‰ (2σ), which is consistent, within uncertainties, with the reported value of 5.39 ± 0.22‰ (Li et al., 2013).

5. Results

5.1. Zircon U-Pb ages

5.1.1. Phin Ngan intrusion

Zircon crystals from the Phin Ngan intrusion are pale brown to colorless, and show stubby prismatic to sub-rounded morphology. Crystal lengths range from 80 to 150 μm, with length/width ratios ranging from 1:1 to 2:1. In CL images, most zircon cores show sector zoning or oscillatory zoning, whereas the rims commonly show patched zoning, cloudy zoning or have high luminescence (Fig. 6).

These textural features are indicative of a magmatic origin for the zircon, but have been modified by later hydrothermal process (Hoskin and Schaltegger, 2003).

Twenty-three spots were measured on the regions that show clear sector zoning or oscillatory zoning. The analyses show moderate to high Th (255–1570 ppm) and U (198–638 ppm) concentrations, with Th/U ratios of 1.2–2.5 (Table 1). Twenty-one concordant analyses cluster together and yield a weighted average ²⁰⁶Pb/²³⁸U age of 824 ± 4 Ma (MSWD = 1.8) (Fig. 7a), which is interpreted as the emplacement age of the Phin Ngan intrusion. Two analyses (PN-02 and PN-23) yield discordant ages, which were probably caused by Pb-loss during later modification event.

5.1.2. Intrusions from the Sin Quyen mine

Three samples from the Sin Quyen mine (SQ-81, SQ-94 and SQ-127) were chosen for zircon U-Pb dating. The zircon grains are pale
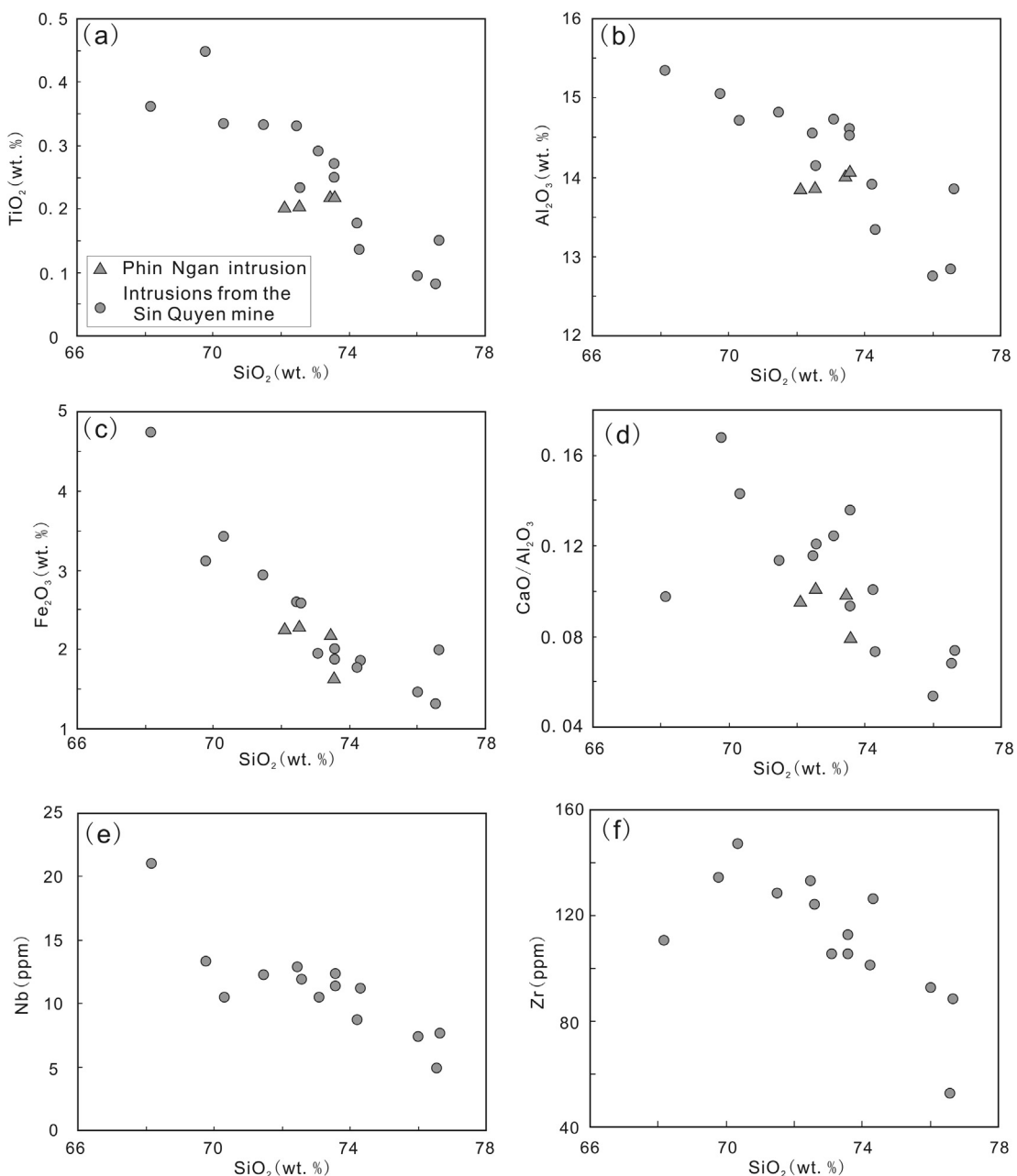

Fig. 8. Plots of (a) TiO₂ vs. SiO₂, (b) Al₂O₃ vs. SiO₂, (c) Fe₂O₃ vs. SiO₂, (d) CaO/Al₂O₃ vs. SiO₂ for the Phin Ngan intrusion and intrusions from the Sin Quyen mine; Plots of (e) Nb vs. SiO₂, and (f) Zr vs. SiO₂ for the intrusions from the Sin Quyen mine.

Table 2
Major oxides (wt.%) and trace elements (ppm) for the granitoids.

	Phin Ngan intrusion				Intrusions from the Sin Quyen mine				
	PN-02	PN-03	PN-06	PN15-01	SQ-05	SQ-06	SQ-07	SQ-08	SQ15-09
SiO$_2$	72.54	73.44	72.11	73.56	74.23	72.58	76.01	76.66	73.57
TiO$_2$	0.21	0.22	0.20	0.22	0.18	0.23	0.09	0.15	0.25
Al$_2$O$_3$	13.88	14.02	13.86	14.08	13.91	14.13	12.75	13.85	14.52
Fe$_2$O$_3$	2.30	2.20	2.27	1.65	1.76	2.58	1.45	1.99	2.01
MnO	0.06	0.06	0.06	0.02	0.05	0.07	0.04	0.05	0.03
MgO	0.30	0.32	0.30	0.33	0.35	0.46	0.72	0.32	0.58
CaO	1.41	1.39	1.33	1.12	1.40	1.71	0.68	1.02	1.35
Na$_2$O	3.05	3.39	3.21	3.27	4.46	3.47	6.10	5.66	4.60
K$_2$O	5.15	5.14	5.40	5.52	2.48	3.95	1.24	2.32	3.94
P$_2$O$_5$	0.05	0.05	0.05	0.05	0.04	0.08	0.02	0.08	0.09
LOI	0.38	0.58	0.31	0.92	0.52	0.42	0.57	0.36	0.50
Total	99.34	100.81	99.10	100.74	99.37	99.68	99.69	102.46	101.44
A/CNK	1.06	1.03	1.02	1.05	1.11	1.08	1.01	1.01	1.02
A/NK	1.31	1.26	1.25	1.24	1.39	1.42	1.12	1.17	1.23
Li	19.1	14.6	15.3	16.8	12.6	20.5	11.9	22.4	29.7
Be	6.27	3.88	5.10	2.52	3.34	2.32	2.40	2.19	2.65
Sc	8.12	8.39	6.49	6.52	5.73	8.29	5.83	6.02	9.42
V	16.7	17.2	14.9	13.3	17.1	20.0	4.17	4.90	20.0
Cr	20.0	20.4	34.1	8.91	23.8	25.1	20.9	27.2	11.6
Co	2.59	3.34	2.74	173	3.94	3.08	2.05	2.39	145
Ni	1.52	1.70	1.91	16.6	4.40	2.87	1.88	5.63	15.6
Cu	3.09	6.91	5.67	3.36	13.3	3.56	1.84	2.91	3.98
Zn	44.2	50.0	50.9	79.9	31.5	56.9	36.5	31.0	60.6
Ga	21.7	22.0	20.4	18.2	16.2	19.4	14.3	16.0	18.1
Rb	244	236	246	271	72.1	140	62.6	99.5	117
Sr	148	145	137	128	151	246	74.2	55.0	225
Y	27.8	27.0	27.0	24.5	27.7	22.2	8.33	7.47	15.8
Zr	184	199	194	213	101	124	92.9	88.5	113
Nb	24.6	24.2	23.7	18.5	8.7	11.9	7.34	7.59	12.3
Cs	1.75	1.52	1.48	1.72	1.23	2.76	2.67	5.20	1.10
Ba	724	706	699	843	428	809	207	265	688
La	52.2	52.1	53.3	51.0	32.5	32.8	30.3	11.8	25.5
Ce	94.2	91.2	92.3	86.4	56.3	62.4	56.7	22.0	45.3
Pr	10.1	9.75	9.94	9.56	6.49	6.91	6.17	2.24	5.65
Nd	31.7	29.6	31.2	30.9	21.1	23.4	18.8	7.6	20.6
Sm	5.25	5.43	5.70	5.38	4.03	4.38	2.97	1.34	4.37
Eu	0.76	0.74	0.72	0.65	0.60	0.70	0.53	0.26	0.78
Gd	4.55	4.30	4.51	4.92	3.72	3.80	2.10	1.12	3.58
Tb	0.75	0.72	0.74	0.80	0.64	0.63	0.29	0.21	0.54
Dy	3.95	3.84	4.00	4.31	3.74	3.33	1.31	1.11	2.78
Ho	0.83	0.80	0.81	0.85	0.80	0.67	0.25	0.23	0.50
Er	2.54	2.38	2.29	2.33	2.47	1.93	0.81	0.66	1.45
Tm	0.38	0.35	0.36	0.36	0.37	0.29	0.11	0.09	0.20
Yb	2.43	2.22	2.14	2.24	2.30	1.79	0.86	0.63	1.43
Lu	0.36	0.34	0.35	0.34	0.36	0.27	0.13	0.10	0.21
Hf	4.78	5.11	4.96	6.04	2.72	3.25	2.62	2.36	3.34
Ta	2.41	2.66	2.53	2.26	0.92	1.00	0.66	0.69	2.00
Pb	9.18	9.15	8.16	17.22	3.09	7.02	1.40	0.90	9.00
Bi	0.01	0.03	0.02	0.05	0.01	0.02	0.01	0.01	0.10
Th	28.7	27.8	29.0	38.9	11.1	12.6	10.2	4.10	11.4
U	6.49	6.79	6.59	9.89	3.84	6.48	1.94	1.37	3.50
(La/Yb)$_N$	15.42	16.86	17.83	16.33	10.1	13.1	25.4	13.5	12.7
Eu∗	0.46	0.45	0.42	0.38	0.47	0.52	0.62	0.63	0.58
Rb/Sr	1.65	1.63	1.80	2.11	0.48	0.57	0.84	1.81	0.52
Sr/Y	5.32	5.38	5.09	5.24	5.47	11.09	8.91	7.36	14.20

Intrusions from the Sin Quyen mine

	SQ15-10	SQ15-11	SQ-16	SQ-54	SQ-80A	SQ-81	SQ-94	SQ-127	SQ-129
SiO$_2$	73.57	73.10	74.33	76.56	68.17	70.32	69.78	72.47	71.48
TiO$_2$	0.27	0.29	0.13	0.08	0.36	0.33	0.45	0.33	0.33
Al$_2$O$_3$	14.61	14.72	13.34	12.83	15.34	14.71	15.04	14.55	14.81
Fe$_2$O$_3$	1.87	1.94	1.85	1.32	4.73	3.43	3.11	2.60	2.94
MnO	0.03	0.04	0.05	0.04	0.06	0.07	0.05	0.06	0.07
MgO	0.51	0.51	0.32	0.19	0.66	0.62	0.87	0.61	0.52
CaO	1.98	1.83	0.98	0.87	1.50	2.10	2.52	1.68	1.68
Na$_2$O	4.21	4.24	3.30	5.07	6.90	3.53	6.69	4.15	3.31
K$_2$O	3.88	3.66	4.88	2.50	1.18	3.54	0.80	3.56	4.14
P$_2$O$_5$	0.10	0.09	0.04	0.02	0.30	0.12	0.16	0.12	0.13
LOI	0.38	0.38	0.59	0.35	0.33	0.54	0.20	0.54	0.35
Total	101.41	100.80	99.80	99.84	99.52	99.32	99.68	100.67	99.77
A/CNK	0.99	1.03	1.07	1.02	1.00	1.09	0.91	1.06	1.14
A/NK	1.31	1.35	1.25	1.16	1.21	1.52	1.27	1.36	1.49

Table 2 (*continued*)

	Phin Ngan intrusion				Intrusions from the Sin Quyen mine				
	PN-02	PN-03	PN-06	PN15-01	SQ-05	SQ-06	SQ-07	SQ-08	SQ15-09
Li	21.3	13.9	6.82	5.88	22.3	20.2	14.0	12.1	13.0
Be	2.66	2.84	3.94	3.90	4.57	4.02	3.56	4.69	4.66
Sc	6.97	7.23	6.74	5.94	17.8	10.1	12.1	8.67	8.99
V	20.0	19.9	7.89	7.76	25.5	31.2	34.3	25.7	27.4
Cr	8.06	9.83	22.2	22.9	21.4	21.7	23.7	19.8	36.7
Co	76.3	78.0	1.78	2.15	9.71	5.08	5.41	3.13	4.09
Ni	7.19	6.58	1.51	1.26	2.53	3.42	3.15	2.44	3.12
Cu	3.60	4.99	3.46	3.48	3.68	6.09	110	4.18	3.47
Zn	49.3	66.7	34.9	38.7	57.2	48.6	29.7	27.2	30.7
Ga	18.8	19.2	15.9	13.6	23.3	20.6	21.0	22.2	20.9
Rb	113	126	117	37.9	66.5	110	39.4	101	129
Sr	253	302	133	152	256	236	182	272	275
Y	21.0	18.6	9.44	20.5	23.7	17.9	13.6	17.2	16.9
Zr	106	105	126	52.9	111	147	135	133	128
Nb	11.3	10.4	11.2	4.86	21.0	10.5	13.3	12.8	12.2
Cs	1.07	1.60	0.74	0.38	2.05	1.54	0.90	1.44	1.79
Ba	709	641	844	701	291	843	186	725	831
La	31.5	27.9	23.0	13.0	26.8	47.2	57.2	31.3	29.5
Ce	60.1	53.4	40.7	24.1	52.5	91.9	107	63.0	57.3
Pr	7.56	6.69	4.70	2.89	5.98	10.8	12.4	7.47	6.68
Nd	27.7	24.9	15.0	10.5	21.8	36.9	40.8	26.3	25.1
Sm	5.98	5.21	2.50	2.29	4.74	6.88	6.81	4.98	4.53
Eu	0.97	0.89	0.48	0.48	0.79	0.87	1.37	0.98	0.85
Gd	5.15	4.26	1.83	2.36	4.32	5.05	4.83	4.00	3.57
Tb	0.75	0.66	0.30	0.46	0.77	0.72	0.66	0.59	0.58
Dy	4.00	3.60	1.49	2.88	4.07	3.34	2.58	2.67	2.76
Ho	0.68	0.63	0.30	0.64	0.73	0.57	0.45	0.52	0.51
Er	1.95	1.91	0.99	1.92	2.04	1.61	1.24	1.47	1.43
Tm	0.30	0.27	0.15	0.29	0.31	0.20	0.14	0.21	0.20
Yb	1.81	1.65	1.06	1.76	2.10	1.40	0.87	1.32	1.35
Lu	0.28	0.27	0.17	0.26	0.26	0.20	0.13	0.19	0.20
Hf	3.19	2.98	3.29	1.67	2.72	3.41	2.94	3.44	3.00
Ta	1.32	1.18	1.09	0.68	1.64	1.01	0.66	1.26	0.99
Pb	8.33	15.3	5.99	9.33	5.09	5.20	8.76	4.44	4.16
Bi	0.05	0.09	0.02	0.02	0.01	0.01	0.09	0.02	0.01
Th	14.0	15.7	8.8	8.11	8.47	11.9	15.8	11.6	11.1
U	3.06	22.8	1.98	3.89	4.22	2.80	0.95	3.31	3.41
$(La/Yb)_N$	12.5	12.1	15.6	5.3	9.2	24.2	47.4	17.0	15.7
Eu*	0.52	0.56	0.66	0.63	0.52	0.43	0.69	0.65	0.63
Rb/Sr	0.45	0.42	0.88	0.25	0.26	0.47	0.22	0.37	0.47
Sr/Y	12.08	16.20	14.11	7.43	10.83	13.22	13.36	15.83	16.24

brown to colorless, and show elongated prismatic morphology. The lengths of zircon grains range from 50 to 120 μm, with length/width ratios of 2:1–4:1. Most grains show well-developed oscillatory zoning in CL images (Fig. 6), consistent with their magmatic origin (Hoskin and Schaltegger, 2003). Few grains show repsorption texture with patched to cloudy zoning, indicating hydrothermal overprint.

Zircon grains from sample SQ-81 contain moderate Th (61–503 ppm) and U (117–685 ppm), with Th/U ratios of 0.2–0.8 (Table 1). All data are distributed on or near concordia, and yield a weighted average $^{206}Pb/^{238}U$ age of 736 ± 8 Ma (MSWD = 5.0) (Fig. 7b). Totally twenty-one grains from sample SQ-94 were analyzed. They have 19–418 ppm Th and 39–916 ppm U, with Th/U ratios of 0.2–0.8 (Table 1). Seventeen concordant/sub-concordant analyses show a coherent cluster, with a weighted average $^{206}Pb/^{238}U$ age of 741 ± 4 Ma (MSWD = 0.29) (Fig. 7c). Three analyses (02, 06, and 10) are obviously discordant, and yield older $^{207}Pb/^{206}Pb$ ages. These analyses were probably conducted on captured zircons from country rocks. One analysis (13) yields a concordant but obviously younger age, which is likely related to later hydrothermal modification process. Zircon grains from sample SQ-127 contain variable Th (43–360 ppm) and U (71–1105 ppm), with Th/U ratios of 0.2–0.9 (Table 1). All data are distributed on or near concordia, and yield a weighted average $^{206}Pb/^{238}U$ age of 758 ± 6 Ma (MSWD = 4.8) (Fig. 7d). Thus, the intrusions from the Sin Quyen mine were formed at 736–758 Ma.

5.2. Whole-rock major and trace elements

Rocks from the Phin Ngan intrusion have uniform major element contents, with high SiO_2 (72.1–73.5 wt.%), K_2O (5.14–5.52 wt.%) and Na_2O (3.05–3.39 wt.%), but low TiO_2 (0.20–0.22 wt.%), Fe_2O_3 (1.65–2.30 wt.%), MgO (0.30–0.33 wt.%) and CaO (1.12–1.41 wt.%) (Fig. 8; Table 2). In the total alkalis *vs.* silica diagram, the compositions fall in the domain of granite, showing sub-alkaline affinity (Fig. 9a). Their A/CNK values range from 1.02–1.06, and A/NK values from 1.24 to 1.31 (Fig. 9b), reflecting weakly peraluminous affinity. Their chondrite-normalized rare earth element (REE) patterns are characterized by right-inclined light REE (LREE) profile ($(La/Eu)_N$ = 16.9–19.1), and nearly flat heavy REE (HREE) profile ($(Gd/Yb)_N$ = 1.6–1.8), with obvious negative Eu anomalies (Eu/Eu* = 0.38–0.46) (Fig. 10a). In the primitive mantle normalized trace element diagram, they show enrichment of large ion lithophile elements (LILE, such as Rb, Th and U), and depletion of Sr, Ba, and high field strength elements (HFSE, such as Nb, Ti and P) (Fig. 10b).

Intrusions from the Sin Quyen mine show large ranges in major element contents (Table 2). Their SiO_2 contents vary from 68.2 to 76.7 wt.%, and total alkali ($K_2O + Na_2O$) from 6.93 to 8.54 wt.%. In the total alkalis *vs.* silica diagram, the compositions are mainly plotted in the domain of granite, showing sub-alkaline affinity (Fig. 9a). They also have wide ranges of TiO_2 (0.08–0.45 wt.%), Al_2O_3 (12.8–15.3 wt.%), Fe_2O_3 (1.32–4.73 wt.%), and CaO

(a)

(b)
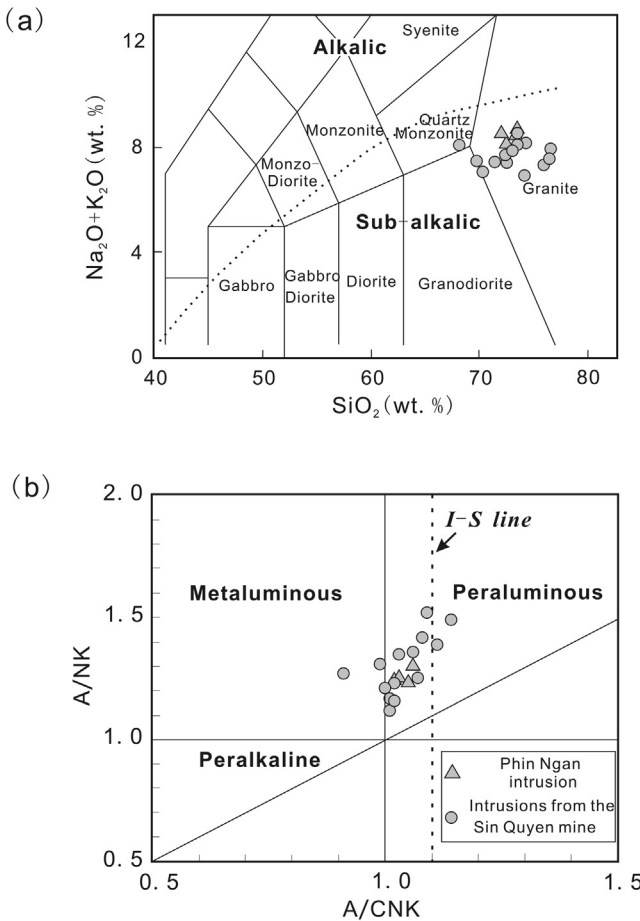
Fig. 9. Plots of (a) SiO_2 vs. $(K_2O + Na_2O)$ and (b) A/NK [molar ratio $Al_2O_3/(Na_2O + K_2O)$] vs. A/CNK [molar ratio $Al_2O_3/(CaO + Na_2O + K_2O)$] for the Phin Ngan intrusion and intrusions from the Sin Quyen mine (after Middlemost, 1994).

(0.68–2.52 wt.%), which are generally linearly correlated with SiO_2 (Table 2; Fig. 8). They have moderate alumina saturation index (A/CNK = 0.91–1.14; A/NK = 1.12–1.52) (Fig. 9b), belonging to metaluminous to weakly peraluminous series. In the chondrite-normalized REE diagram, all samples are marked by right-inclined LREE profile $((La/Eu)_N = 6.6–14.0)$ and nearly flat HREE profile $((Gd/Yb)_N = 1.1–4.6)$, with moderate to strong negative Eu anomalies $(Eu/Eu^* = 0.43–0.69)$ (Fig. 10c). They have primitive mantle-normalized patterns enriched in LILE (e.g., Rb, Th and U), and depleted in HFSE (e.g., Nb, Ti, and P) (Fig. 10d). Some samples show obvious depletion in Sr and Ba (Fig. 10d).

5.3. Whole-rock Sm-Nd isotopes

The whole-rock Sm-Nd isotopic data are listed in Table 3 and are illustrated in Fig. 11a. Rocks from the Phin Ngan intrusion have ε_{Nd} values ranging from −8.4 to −5.2 at 824 Ma. Compared with the Phin Ngan intrusion, intrusions from the Sin Quyen mine generally have higher and more scattered ε_{Nd} values (−6.6 to 0 at 750 Ma). The Sm-Nd isotopic compositions of meta-sedimentary rocks from the Sin Quyen Group were also analyzed as they are the represents of basement rocks in the region. The meta-sedimentary rocks have ε_{Nd} values ranging from −7.8 to −6.7 at 750 Ma.

5.4. In-situ zircon Lu-Hf and O isotopes

In-situ zircon Lu-Hf and O isotopic data are listed in Table 4 and are illustrated in Fig. 11b. Zircon grains from the Phin Ngan intru-

sion (PN-01) have a narrow range of initial $^{176}Hf/^{177}Hf$ values (0.282029–0.282101), corresponding to relatively uniform $\varepsilon_{Hf}(t)$ values (−8.1 to −5.5). They also have a narrow range of $\delta^{18}O$ values (9.7–10.9‰).

Two samples from the Sin Quyen mine (SQ-127 and SQ-81) were selected for zircon Lu-Hf and O isotope analysis. Zircon grains from sample SQ-127 have $\varepsilon_{Hf}(t)$ values varying from −6.7 to −2.3 and $\delta^{18}O$ values from 7.3 to 12.4‰. The grains with higher $\varepsilon_{Hf}(t)$ values tend to have lower $\delta^{18}O$ values. Zircon grains from sample SQ-81 have highly scattered $\varepsilon_{Hf}(t)$ values (−6.6 to +11.1) and $\delta^{18}O$ values (4.3–10.2‰).

6. Discussion

6.1. Petrogenesis

6.1.1. Phin Ngan intrusion

Granitoids can be commonly produced by differentiation of mantle-derived mafic magmas, as indicated by the classic "basalt-andesite-dacite-rhyolite series" (Grove et al., 1982; Mann, 1983; Ewart and Hawkesworth, 1987), by mixing of mantle-derived mafic magma with crust-derived felsic magma (e.g., Castro et al., 1991; Kemp et al., 2007; Karsli et al., 2010), or by partial melting of rocks in middle-lower crust (e.g., Roberts and Clemens, 1993; Chappell et al., 2012).

Some ∼815 Ma mafic intrusions have been identified in the Ailao Shan-Pan Si Pan belt (Cai et al., 2014). These mafic rocks are the only mantle-derived materials that could possibly represent the parental magmas of the Phin Ngan intrusion. However, the Phin Ngan intrusion has $\varepsilon_{Nd}(t)$ values (−8.4 to −5.2) obviously lower than those of mafic rocks (−3.5 to +4.4), suggesting that they were derived from different magma sources. In addition, the Phin Ngan intrusion has zircon $\delta^{18}O$ values (9.7–10.9‰) obviously higher than those of mantle-derived magmas (5.3 ± 0.6‰; Valley et al., 2005). Therefore, the Phin Ngan intrusion cannot be differentiation products of the mantle-derived magmas. The granitoids produced through magma mixing are normally characterized by the occurrence of mafic enclaves and a wide range of geochemical compositions. However, no mafic enclaves can be observed in the Phin Ngan intrusion, and the Phin Ngan intrusion has relatively constant mineral assemblage and geochemical composition. These evidences rule out the possibility that the Phin Ngan intrusion was produced by magma mixing.

We note that the Phin Ngan intrusion contains high and fairly uniform SiO_2 and K_2O, and low MgO and Fe_2O_3, suggesting that it may have been produced by partial melting of crustal materials at depth. Experimental studies demonstrate that the content of K in a magma source has a significant influence on the composition of derived magma. For example, meta-tholeiitic rocks have low contents of K_2O, and cannot yield high-K calc-alkaline melts (Roberts and Clemens, 1993). In contrast, melting of medium- to high-K rocks, such as high-K basalt, can generate a peraluminous melt with high K content (e.g., Sisson et al., 2005). It is also found that dehydration melting of hydrous mineral-bearing mafic rocks yield water-undersaturated mildly peraluminous granodioritic melts (Beard and Lofgren, 1991; Wolf and Wyllie, 1994), whereas water-saturated melting of these rocks commonly generated strong peraluminous melts (Beard and Lofgren, 1991). The Phin Ngan intrusion has high K_2O contents and moderate A/CNK values. Thus, it was most probably generated by dehydration melting of high-K rocks at depth. The Phin Ngan intrusion has similar whole-rock two-stage Nd model ages (2.04–2.19 Ga) and zircon two-stage Hf model ages (2.07–2.23 Ga), implying that the source materials have residential ages up to 2.2 Ga. The high zircon $\delta^{18}O$ values (9.7–10.9‰) indicate that the source rocks have
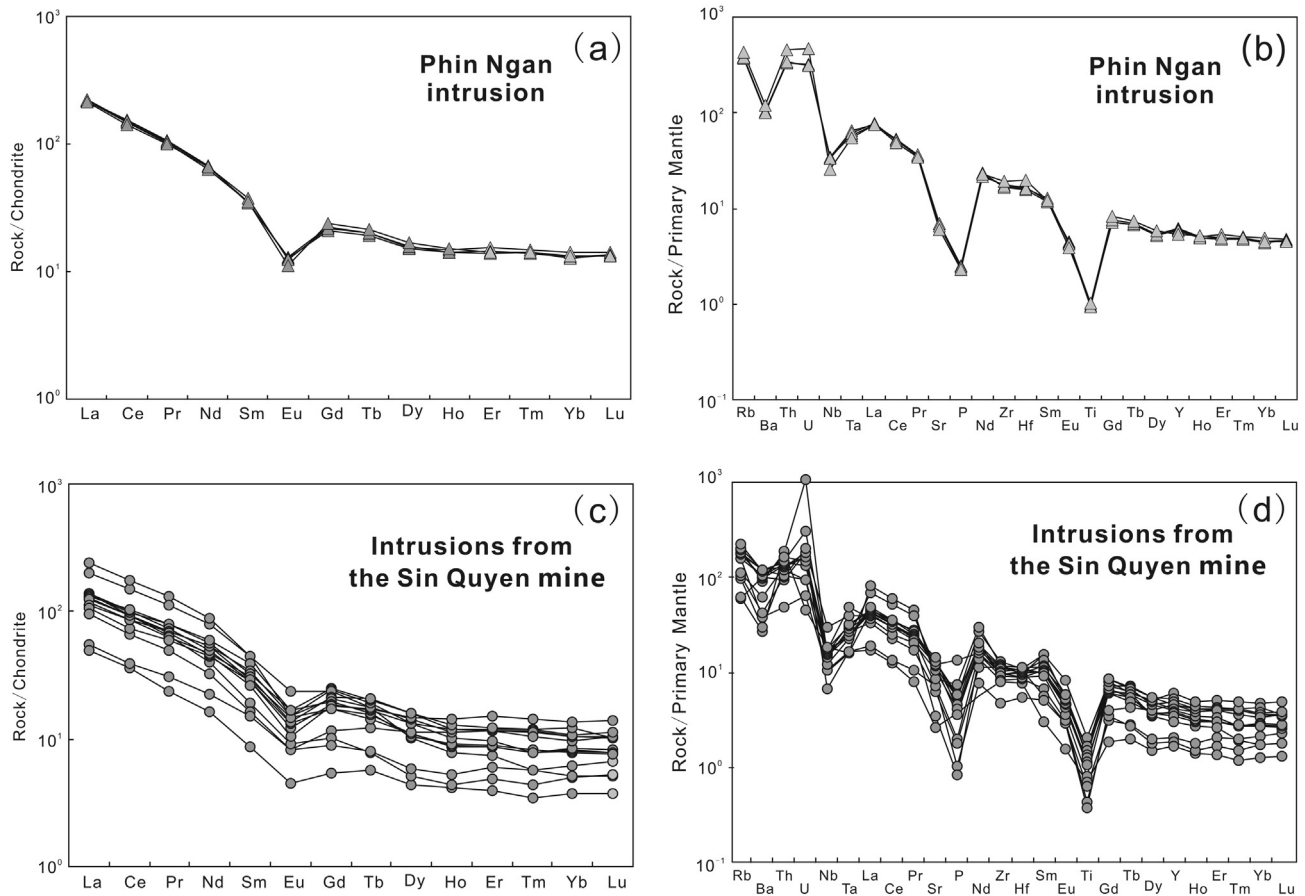
Fig. 10. Chondrite-normalized REE patterns for the (a) Phin Ngan intrusion and (c) intrusions from the Sin Quyen mine. Primitive mantle (PM) normalized trace element patterns for the (b) Phin Ngan intrusion and (d) intrusions from the Sin Quyen mine. The Chondrite values and PM values are from Sun and McDonough (1989).

Table 3
Sm-Nd isotopic data for the Phin Ngan intrusions, intrusions from the Sin Quyen mine and meta-sedimentary basement rocks.

Rocks	Sample name	Sm(ppm)	Nd(ppm)	$^{147}Sm/^{144}Nd$	$^{143}Nd/^{144}Nd$	2σ	$\varepsilon_{Nd}(t)$	$T_{DM1}(Ga)$	$T_{DM2}(Ga)$
Phin Ngan intrusion	PN-03	5.43	29.6	0.1149	0.511767	0.000036	−8.4	2.13	2.19
	PN-04	16.4	99.9	0.1032	0.511841	0.000014	−5.7	1.80	2.07
	PN-05	15.8	98.6	0.1007	0.511855	0.000019	−5.2	1.75	2.04
Intrusions from the Sin Quyen mine	SQ-05	4.03	21.1	0.1198	0.512016	0.000037	−4.8	1.84	1.81
	SQ-06	4.38	23.4	0.1177	0.512030	0.000030	−4.3	1.78	1.78
	SQ-80	4.74	21.8	0.1364	0.512006	0.000031	−6.6	2.25	1.84
	SQ-81	6.88	36.9	0.1169	0.512245	0.000028	0.0	1.43	1.44
	SQ-127A	4.98	26.3	0.1189	0.511968	0.000044	−5.6	1.90	1.88
	SQ-129A	4.53	25.1	0.1133	0.511975	0.000049	−4.9	1.78	1.87
Meta-sedimentary basement rocks	SQ14-12	8.33	43.9	0.1190	0.511911	0.000043	−6.7	1.99	1.97
	SQ14-14	10.4	54.8	0.1190	0.511857	0.000035	−7.8	2.08	2.06
	SQ14-15	6.54	36.8	0.1116	0.511862	0.000035	−7.0	1.92	2.04

Note: The $\varepsilon_{Nd}(t)$ values have been calculated at 825 Ma for the Phin Ngan intrusion, and 750 Ma for the intrusions from the Sin Quyen mine and meta-sedimentary basement rocks.

experienced some surface processes, such as low-temperature alteration and chemical weathering (Valley et al., 2005). We note that the Phin Ngan intrusion has low contents of CaO (1.1–1.4 wt.%), and displays obvious Ba and Sr depletions in the primitive mantle-normalized trace element diagram and negative Eu anomalies in the chondrite-normalized REE patterns, implying that plagioclase fractionation may have occurred in the magma evolution process. Collectively, the Phig Ngan was produced by dehydration melting of ancient, high-K crustal rocks, probably followed by fractional crystallization of plagioclase.

6.1.2. Intrusions from the Sin Quyen mine

Some mantle-derived mafic intrusions (∼770 Ma) broadly contemporaneous to the intrusions from the Sin Quyen mine occur in the Ailao Shan-Phan Si Pan belt (Qi et al., 2012), but there are no spatial relationships between them. In addition, intrusions from the Sin Quyen mine have zircon $\delta^{18}O$ values different from those of typical mantle-derived magma (Fig. 11b), suggesting that they were not produced simply by differentiation of mantle-derived magmas.

Intrusions from the Sin Quyen mine have high SiO_2 and total alkali ($K_2O + Na_2O$), and low MgO, Cr and Ni, suggesting that their
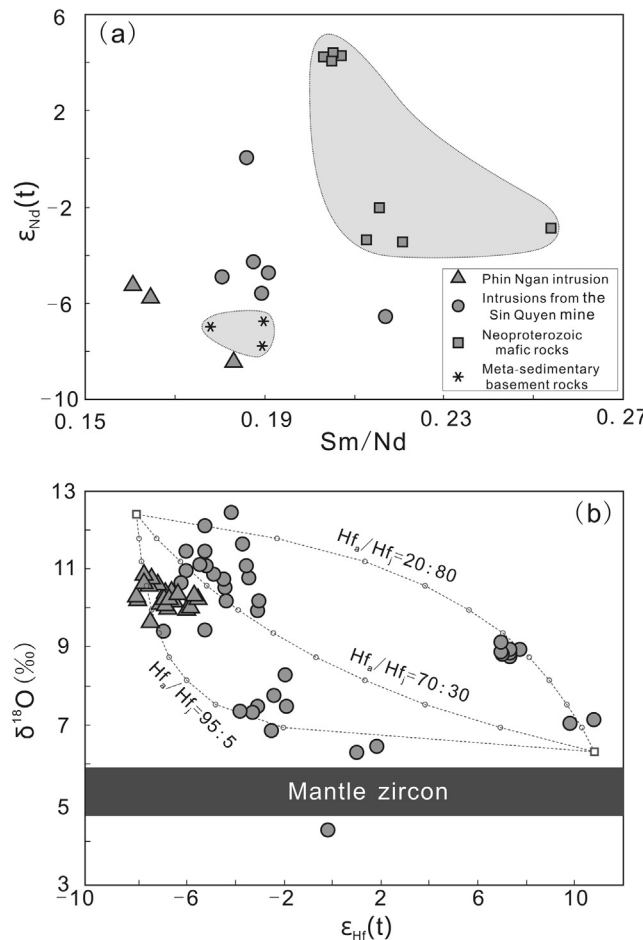
Fig. 11. (a) Plot of Sm/Nd *vs.* $\varepsilon_{Nd}(t)$ for the Phin Ngan intrusion and intrusions from the Sin Quyen mine. The data for meta-sedimentary basement rocks and regional mantle-derived mafic intrusions (Cai et al., 2014) are also shown for comparison. (b) Plot of zircon $\varepsilon_{Hf}(t)$ *vs.* $\delta^{18}O$ values for the Phin Ngan intrusion and intrusions from the Sin Quyen mine. The dotted lines denote two-component mixing trends between the ancient crust-derived and mantle-/juvenile crust-derived magmas. With negligible magma mixing taken into consideration, it is assumed that the lowest $\varepsilon_{Hf}(t)$ value (-8.1) and highest $\delta^{18}O$ value (12.4) we obtained represent the composition of ancient crust-derived magma, and the highest $\varepsilon_{Hf}(t)$ (10.8) and relatively low $\delta^{18}O$ value (6.3) represent that of mantle-/juvenile crust-derived magma. Hf_a/Hf_j is the ratio of Hf concentration in the ancient crust-derived magma (a) over mantle-/juvenile crust-derived magma (j) indicated for each curves. The small open circles on the curves represent 10% mixing increments.

parental magmas were mainly from crustal sources. They have wide ranges of whole-rock major and trace elemental compositions, and whole-rock Nd and zircon Hf-O isotopic compositions (Figs. 8, 10 and 11), precluding simple crystal-liquid fractionation of a common parental magma to generate the entire suite. Such variable compositions indicate isotope disequilibrium in the magma chamber which may have resulted from magma mixing or wallrock assimilation (e.g., Kemp et al., 2007; Appleby et al., 2008). The intrusions from the Sin Quyen mine mainly have negative whole-rock $\varepsilon_{Nd}(t)$ values (−6.6 to −4.3), with two-stage Nd model ages varying from 1.78 to 1.88 Ga. Most zircon grains have low $\varepsilon_{Hf}(t)$ values (−6.9 to −2.2) and high $\delta^{18}O$ values (up to +12.4‰). Thus, these intrusions should have been mainly derived from partial melting of ancient crustal rocks that had experienced some surface processes. Some zircon grains have high $\varepsilon_{Hf}(t)$ (up to +11.1) and relatively low $\delta^{18}O$ values. Besides, sample SQ-81 has $\varepsilon_{Nd}(t)$ value (0) obviously higher than those of meta-sedimentary basement rocks but approaching those of mantle-derived mafic rocks (Fig. 11a). These isotopic data indicate that mantle- or juvenile crustal-derived melts were variably involved in the magma

petrogenesis through magma mixing or assimilation. Considering that all but one zircon grains have $\delta^{18}O$ values higher than those of mantle-derived magmas, juvenile crustal-derived components are the more likely candidates incorporated into the magma chamber. One zircon grain has $\delta^{18}O$ value lower than the mantle range (Fig. 11b), which was probably related to local high-temperature alteration process (Valley et al., 2005).

Fractional crystallization also occurred in the generation of the intrusions from the Sin Quyen mine, and may partially account for their compositional variations. For example, the decreasing CaO/Al_2O_3 ratios with increasing SiO_2 (Fig. 8d), negative Eu anomalies in the chondrite-normalized REE patterns (Fig. 10c), and Ba-Sr depletions in the primitive mantle-normalized trace element diagram (Fig. 10d) are consistently indicative of plagioclase fractionation in the magma evolution process. This is in compatible with the occurrence of euhedral plagioclase aggregates in some samples (Fig. 5h). Titanium- and Nb-bearing minerals (e.g., ilmenite, titanite) might be other fractionated phases, given the presence of titanite in some samples and the decreasing TiO_2 and Nb with increasing SiO_2 (Figs. 8a and e). Zircon fractionation may also occur as indicated by the negative correlation between Zr and SiO_2 (Fig. 8f). In summary, intrusions from the Sin Quyen mine were mainly produced through partial melting of ancient crustal rocks, followed by variable magma mixing/wallrock assimilation and fractional crystallization during the magma evolution process.

6.2. Geodynamic setting

The Phin Ngan intrusion and intrusions from the Sin Quyen mine are sub-alkaline in nature, and show geochemical features of arc-affinity, i.e., enrichment of LILE (e.g., Rb, Th and U) and LREE, but depletion of HFSE (e.g., Nb, Ti and P). The broadly contemporaneous mantle-derived mafic intrusions in the region, including the 803 Ma Jinping amphibolites and 769 Ma Daping hornblende-gabbro, show similarly arc-like geochemical signatures (Qi et al., 2012; Cai et al., 2014). In the tectonic discrimination diagrams for granitoids, most Neoproterozoic granitoids in the Ailao Shan-Phan Si Pan belt fall within the field of volcanic arc granitoid (Fig. 12). Thus, the Neoproterozoic intrusions in the Ailao Shan-Phan Si Pan belt have been proposed to be generated in a subduction-related setting (Qi et al., 2012, 2014; Cai et al., 2014, 2015). Admittedly, the subduction-related geochemical features alone cannot distinguish subduction-related magmatic rocks from rocks derived from pre-existing subduction-related materials, but it is notable that the Neoproterozoic magmatism in the Ailao Shan-Phan Si Pan belt is characterized by abundant sub-alkaline, felsic rocks (e.g., diorite, granodiorite, adakitic granite, K-rich granite) and subordinate mafic rocks, without alkaline rocks or S-type granites. This rock association is also typical for a subduction-related setting (Barbarin, 1999).

The Phin Ngan intrusion and intrusions from the Sin Quyen mine have low Sr/Y (5.1–16.2) and (La/Yb)$_N$ (5.3–47.4) ratios (Table 2), and display flat HREE patterns (Fig. 10), implying no residual garnet in their magma sources, i.e., partial melting occurred under moderate to low pressures (<12 kbar) (Green, 1994; Foley et al., 1996). Anatexis of crustal materials to generate granitic melts under relatively low pressures commonly need external heat input, such as mantle upwelling or mafic magma emplacement (Petford and Gallagher, 2001). The occurrence of broadly coeval mafic intrusions in the region implies that the mafic magmatism probably provided necessary heat for crust melting. Crust anatexis induced by mafic magma underplating or intraplating is usually related to extension or transtensional processes (e.g., Zhou et al., 2006; Collins and Richards, 2008; Kemp et al., 2009). Thus, the Phin Ngan intrusion and intrusions from the Sin Quyen mine may have been emplaced in a subduction-related extensional setting, such as the waning

Table 4

In-situ Hf and O isotopic compositions for zircon from the Phin Ngan intrusion and intrusions from the Sin Quyen mine.

	t (Ma)	$^{176}Yb/^{177}Hf$	$^{176}Lu/^{177}Hf$	$^{176}Hf/^{177}Hf$	2σ	$^{176}Hf/^{177}Hf_i$	εHf(t)	T_{DM1}(Ga)	T_{DM2}(Ga)	$\delta^{18}O$	2σ
Phin Ngan intrusion											
PN-01-01	824	0.014773	0.000589	0.282086	0.000021	0.282077	−6.4	1.63	2.12	10.4	0.4
PN-01-02	824	0.004543	0.000191	0.282048	0.000015	0.282045	−7.5	1.66	2.19	10.6	0.3
PN-01-03	824	0.010713	0.000425	0.282094	0.000022	0.282088	−6.0	1.61	2.10	10.0	0.2
PN-01-04	824	0.013070	0.000508	0.282075	0.000019	0.282067	−6.7	1.64	2.14	10.3	0.3
PN-01-05	824	0.017600	0.000640	0.282074	0.000019	0.282064	−6.9	1.64	2.15	10.1	0.3
PN-01-06	824	0.013649	0.000529	0.282070	0.000019	0.282062	−6.9	1.64	2.15	10.3	0.3
PN-01-07	824	0.012726	0.000520	0.282037	0.000018	0.282029	−8.1	1.69	2.23	10.3	0.4
PN-01-08	824	0.011943	0.000476	0.282079	0.000017	0.282071	−6.6	1.63	2.13	10.5	0.3
PN-01-09	824	0.014566	0.000569	0.282101	0.000020	0.282093	−5.9	1.60	2.08	10.1	0.3
PN-01-10	824	0.014468	0.000564	0.282055	0.000018	0.282046	−7.5	1.67	2.19	10.8	0.4
PN-01-11	824	0.016711	0.000653	0.282079	0.000021	0.282069	−6.7	1.64	2.14	10.3	0.2
PN-01-12	824	0.010945	0.000425	0.282045	0.000016	0.282038	−7.8	1.68	2.21	10.7	0.3
PN-01-13	824	0.010869	0.000448	0.282052	0.000017	0.282045	−7.5	1.67	2.19	9.7	0.3
PN-01-14	824	0.017499	0.000659	0.282108	0.000020	0.282097	−5.7	1.60	2.07	10.4	0.3
PN-01-15	824	0.018387	0.000687	0.282085	0.000034	0.282074	−6.5	1.63	2.13	10.2	0.2
PN-01-16	824	0.010294	0.000375	0.282061	0.000029	0.282055	−7.2	1.65	2.17	10.7	0.3
PN-01-17	824	0.012020	0.000450	0.282046	0.000031	0.282039	−7.8	1.68	2.20	10.9	0.3
PN-01-18	824	0.014624	0.000548	0.282039	0.000030	0.282031	−8.0	1.69	2.22	10.3	0.3
PN-01-19	824	0.013485	0.000516	0.282071	0.000026	0.282063	−6.9	1.64	2.15	10.4	0.3
PN-01-20	824	0.008468	0.000313	0.282063	0.000021	0.282058	−7.1	1.65	2.16	10.2	0.3
PN-01-21	824	0.016417	0.000630	0.282111	0.000021	0.282101	−5.5	1.59	2.07	10.3	0.4
PN-01-22	824	0.014558	0.000559	0.282075	0.000020	0.282067	−6.8	1.64	2.14	10.0	0.3
Intrusions from the Sin Quyen mine											
SQ-127-01	750	0.027301	0.001067	0.282255	0.000015	0.282240	−2.3	1.41	1.80	7.4	0.3
SQ-127-02	750	0.003324	0.000105	0.282117	0.000015	0.282116	−6.7	1.56	2.08	10.6	0.3
SQ-127-03	750	0.018934	0.000736	0.282178	0.000014	0.282167	−4.9	1.51	1.97	10.5	0.3
SQ-127-04	750	0.016123	0.000601	0.282197	0.000018	0.282188	−4.1	1.47	1.92	11.6	0.2
SQ-127-05	750	0.008222	0.000275	0.282170	0.000014	0.282166	−4.9	1.50	1.97	10.7	0.2
SQ-127-06	750	0.021469	0.000819	0.282156	0.000017	0.282144	−5.7	1.54	2.02	12.1	0.3
SQ-127-07	750	0.019843	0.000709	0.282217	0.000016	0.282207	−3.4	1.45	1.88	10.2	0.4
SQ-127-08	750	0.011755	0.000396	0.282198	0.000015	0.282192	−4.0	1.46	1.91	11.1	0.3
SQ-127-09	750	0.050819	0.001866	0.282264	0.000018	0.282238	−2.4	1.43	1.81	8.3	0.4
SQ-127-10	750	0.012620	0.000430	0.282211	0.000016	0.282205	−3.5	1.45	1.88	9.9	0.5
SQ-127-11	750	0.038850	0.001446	0.282220	0.000020	0.282200	−3.7	1.47	1.89	7.3	0.2
SQ-127−12	750	0.020056	0.000704	0.282164	0.000017	0.282154	−5.3	1.52	2.00	10.9	0.4
SQ-127-13	750	0.022167	0.000880	0.282156	0.000023	0.282144	−5.7	1.54	2.02	11.5	0.2
SQ-127-14	750	0.036487	0.001347	0.282142	0.000023	0.282123	−6.4	1.58	2.07	11.0	0.4
SQ-127-15	750	0.013604	0.000471	0.282202	0.000023	0.282196	−3.9	1.46	1.90	10.8	0.3
SQ-127-16	750	0.002868	0.000089	0.282147	0.000024	0.282146	−5.6	1.52	2.01	11.1	0.2
SQ-127-17	750	0.036994	0.001395	0.282245	0.000024	0.282225	−2.8	1.44	1.84	7.7	0.5
SQ-127-18	750	0.018045	0.000631	0.282132	0.000022	0.282123	−6.4	1.56	2.06	11.5	0.3
SQ-127-19	750	0.003896	0.000123	0.282140	0.000021	0.282138	−5.9	1.53	2.03	11.1	0.3
SQ-127-20	750	0.022451	0.000815	0.282187	0.000029	0.282175	−4.6	1.50	1.95	12.4	0.4
SQ-81-01	750	0.038429	0.001407	0.282328	0.000019	0.282308	0.1	1.32	1.65	4.3	0.3
SQ-81-02	750	0.044864	0.001727	0.282615	0.000017	0.282591	10.1	0.92	1.02	7.0	0.4
SQ-81-03	750	0.000649	0.000019	0.282521	0.000014	0.282521	7.7	1.01	1.17	8.7	0.3
SQ-81-04	750	0.035161	0.001351	0.282636	0.000021	0.282617	11.1	0.88	0.96	7.1	0.3
SQ-81-05	750	0.036241	0.001365	0.282225	0.000019	0.282206	−3.5	1.46	1.88	7.3	0.3
SQ-81-06	750	0.025705	0.000955	0.282240	0.000016	0.282227	−2.7	1.43	1.83	7.5	0.3
SQ-81-07	750	0.000535	0.000015	0.282533	0.000016	0.282533	8.1	0.99	1.15	8.9	0.3
SQ-81-08	750	0.000418	0.000011	0.282510	0.000015	0.282510	7.3	1.02	1.20	9.1	0.2
SQ-81-09	750	0.056626	0.002130	0.282195	0.000018	0.282165	−4.9	1.54	1.97	9.4	0.2
SQ-81-10	750	0.000979	0.000031	0.282521	0.000017	0.282521	7.7	1.01	1.17	8.9	0.3
SQ-81-11	750	0.000277	0.000008	0.282511	0.000016	0.282511	7.3	1.02	1.20	8.8	0.3
SQ-81-12	750	0.010755	0.000334	0.282121	0.000023	0.282117	−6.6	1.57	2.08	9.4	0.4
SQ-81-13	750	0.025811	0.000887	0.282355	0.000022	0.282342	1.3	1.26	1.58	6.3	0.4
SQ-81-14	750	0.000645	0.000018	0.282512	0.000018	0.282512	7.4	1.02	1.19	8.8	0.2
SQ-81-15	750	0.043811	0.001591	0.282212	0.000026	0.282190	−4.1	1.49	1.92	10.2	0.3
SQ-81-16	750	0.036135	0.001440	0.282263	0.000023	0.282243	−2.2	1.41	1.80	6.8	0.3
SQ-81-17	750	0.030343	0.001058	0.282380	0.000035	0.282365	2.1	1.24	1.52	6.4	0.4
SQ-81-18	750	0.007137	0.000222	0.282523	0.000036	0.282520	7.6	1.01	1.18	8.8	0.3

Note: The εHf(t) values have been calculated at 825 Ma for the Phin Ngan intrusion, and 750 Ma for the intrusions from the Sin Quyen mine.

stage of subduction, hiatus of the continuous subduction due to the slab rollback or change of subduction motion.

6.3. Tectonic linkage between Northwest Vietnam and the Yangtze Block

As mentioned above, Northwest Vietnam has been tectonically attributed to either Indochina (e.g., Qi et al., 2012, 2014) or South China Blocks (e.g., Chung et al., 1997; Zelazniewicz et al., 2013). The Neoproterozoic igneous rocks in this belt may provide constraints on this issue. The synthesis of available age data shows an age-range of ∼740 to ∼840 Ma for the Neoproterozoic igneous activity in the Ailao Shan-Phan Si Pan belt (Fig. 2), which just falls within the overall age-range (710–870 Ma) of prolonged magmatic activity along the margin of the Yangtze Block of South China (Zhao and Cawood, 2012 and references therein). Detrital zircons from
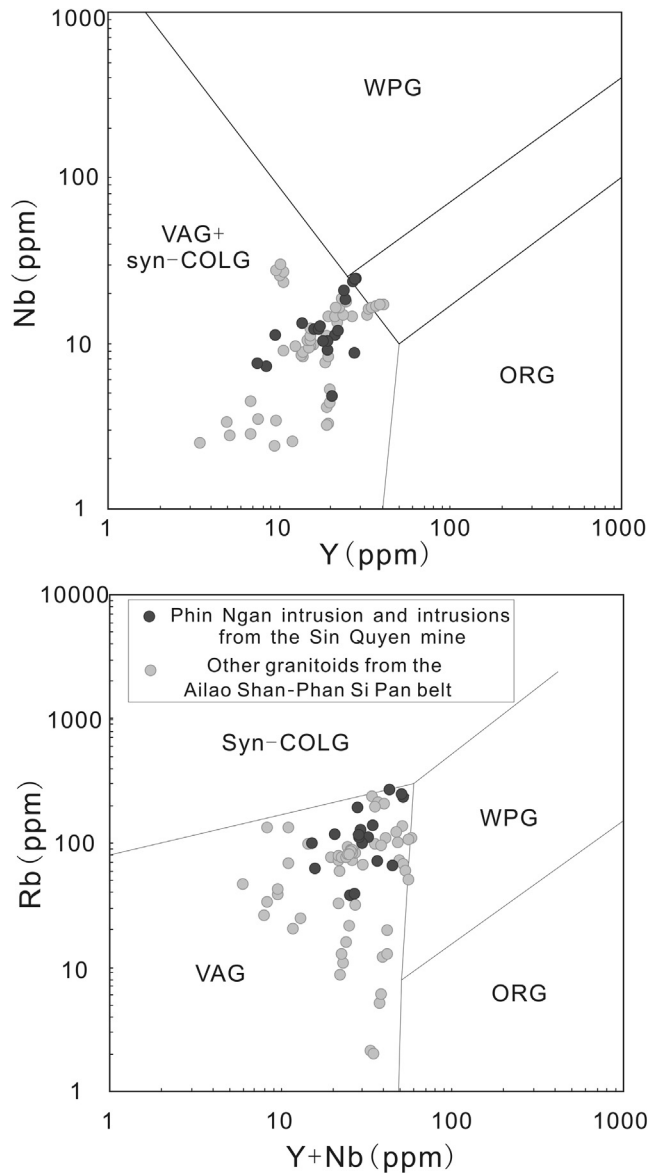
Fig. 12. Plot of (a) Y *vs.* Nb and (b) (Y + Nb) *vs.* Rb for the granitoids in the Ailao Shan-Phan Si Pan belt. The intrusions include Posen granite (Lan et al., 2000; Pham et al., 2009); Daping granodiorite (Qi et al., 2012); Jinzhoulin, Leidashu, Chaojiagou and Zhetai granitoids, (Qi et al., 2014); Adebo quartz diorite (Cai et al., 2015); Phin Ngan intrusion (this study); and intrusions from the Sin Quyen mine (this study). The tectonic classification is suggested by Pearce et al., (1984). Syn-COLG = syn-collisional granite; WPG = within plate granite; ORG = orogenic granites; and VAG = volcanic arc granite.

river sediment samples in the Truong Son Belt of the Indochina Block show dominant Neoarchean (∼2.5 Ga), Mesoproterozoic (1.7–1.4 Ga), Grenvillian (∼0.95 Ga), and Pan-African (0.65– 0.5 Ga) age spectrums, notably without Neoproterozoic age peaks (Usuki et al., 2013). In this aspect, Northwest Vietnam may maintain a tectonic affinity with the Yangtze Block of South China rather than the Indochina Block.

In the southeastern Yangtze Block, the Neoproterozoic magmatism is characterized by abundant S-type and I-type granitoids, and minor mafic-ultramafic rocks (e.g., Wang et al., 2006, 2013; Wang et al., 2007a,b; Zheng et al., 2007, 2008; Zhang et al., 2012, Zhang and Wang, 2016). This rock association is different from that of Ailao Shan-Phan Si Pan belt. In contrast, abundant sub-alkaline, I-type granitoids and subordinate mafic and intermediate rocks occur in the western margin of the Yangtze Block (e.g., Zhou
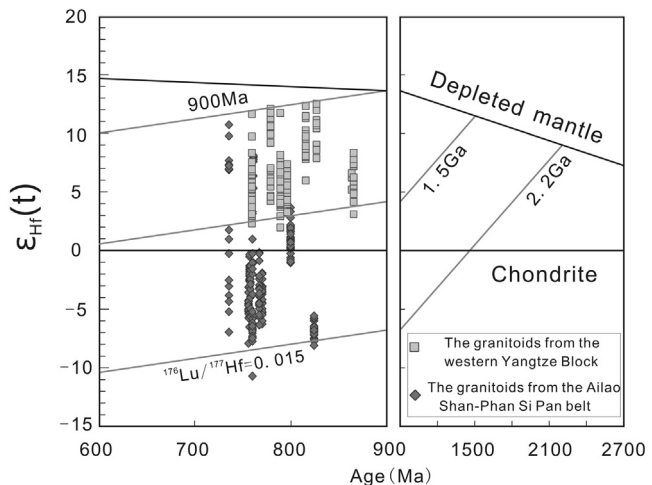
Fig. 13. Schematic diagram for zircon U-Pb age *vs.* $\varepsilon_{Hf}(t)$ for granitoids in the Ailaoshan-Phan Si Pan belt and western margin of the Yangtze Block. Reference lines representing meteoritic Hf evolution (CHUR) and depleted mantle are from Blichert-Toft and Albarede (1997) and Griffin et al. (2000), respectively. The Hf isotope data for granitoids in the Ailaoshan-Phan Si Pan belt are from Pham et al., (2009), Qi et al., (2012, 2014), Cai et al., (2015) and this study; those for granitoids in the western Yangtze Block are from Zhao et al. (2008) and Zhao and Zhou (2008), Huang et al., (2008, 2009), and Chen et al., (2015).

et al., 2002; Li et al., 2003; Chen et al., 2015; Zhao et al., 2011), which is similar to the rock association in the Ailao Shan-Phan Si Pan belt. As the Neoproterozoic igneous rocks along the western margin of the Yangtze Block has been considered to define a super-subduction system (e.g., Zhou et al., 2002; Zhao et al., 2011), that in the Ailao Shan-Phan Si Pan belt most probably represents the southeastern extension part of this system. It is notable that the Neoproterozoic granitoids in the Ailao Shan-Phan Si Pan belt generally have negative zircon $\varepsilon_{Hf}(t)$ values, i.e., they were mainly sourced from Meso- to Paleoproterozoic crust; whereas those along the western margin of the Yangtze Block mainly have positive zircon $\varepsilon_{Hf}(t)$ values, i.e., they were derived from juvenile continental crust or oceanic crust (Fig. 13). This contrast can be partially attributed to the different ages of basement rocks in the two regions: Paleoproterozoic (>1.7 Ga) basement rocks are widespread in the Ailao Shan-Phan Si Pan belt (Pham et al., 2012; Wang et al., 2016), whereas late Mesoproterozoic to early Neoproterozoic (<1.0 Ga) basement rocks are dominant in the western margin of the Yangtze Block (e.g., Sun et al., 2009; Zhu et al., 2016).

We also note that the mafic-ultramafic rocks in the Song Da rift have ages and geochemical compositions similar to the Permian flood basalts in the Emeishan Large Igneous Province (ELIP) of the western Yangtze Block (Wang et al., 2007a,b; Anh et al., 2011). The felsic volcanic rocks in the Tu Le basin have temporal, petrographic, and geochemical characteristics similar to those in the inner zone of the ELIP as well (Usuki et al., 2015). Therefore, the Song Da-Tu Le region is considered to represent a southeastward displaced portion of the ELIP (Tran et al., 2015; Usuki et al., 2015). Furthermore, the Cam Duong Formation distributed along the right bank of the Red River is composed of hundreds of meters of phosphorite-bearing sediments. Siltstones and schist from this formation contain acritach assemblage of early Cambrian age. It is suggested that the Cam Duong Formation can be well comparable with the Cambrian phosphorite-bearing Meishucun Formation in the southwestern Yangtze Block (Yue et al., 2013). In summary, all these geological coincidences imply that Northwest Vietnam represents a southeastward displaced part of the western Yangtze Block along the ASRR shear zone, i.e., the southeastern portion of the boundary between the South China and Indochina Blocks is the Song Ma belt rather than the Red River fault zone.

7. Conclusions

Several granitic intrusions have been studied in the Phan Si Pan belt, Northwest Vietnam, including the ~825 Ma Phin Ngan intrusion, and the ~760 to ~740 Ma granitic dykes or stocks from the Sin Quyen mine. The Phin Ngan intrusion was generated by partial melting of ancient, high-K crustal rocks. Granitic intrusions from the Sin Quyen mine were mainly derived from partial melting of ancient crustal rocks, with subordinate contributions from mantle-/juvenile crust-derived components. These granitoids were formed in a subduction-related setting, which matches well with the Neoproterozoic subduction-related igneous rocks along the western margin of the Yangtze Block in South China. This magmatic correlation, together with other related geological coincidences, indicates that Northwest Vietnam represents a southeastward displaced part of the Yangtze Block along the ASRR shear zone.

Acknowledgements

References

Anh, T.V., Pang, K.N., Chung, S.L., Lin, H.M., Hoa, T.T., Anh, T.T., Yang, H.J., 2011. The Song Da magmatic suite revisited: a petrologic, geochemical and Sr–Nd isotopic study on picrites, flood basalts and silicic volcanic rocks. J. Asian Earth Sci. 42, 1341–1355.

Appleby, S.K., Graham, C.M., Gillespie, M.R., Hinton, R.W., Oliver, G.J.H., EIMF, 2008. A cryptic record of magma mixing in diorites revealed by high-precision SIMS oxygen isotope analysis of zircons. Earth Planet. Sci. Lett. 269, 105–117.

Barbarin, B., 1999. A review of the relationships between granitoid types, their origins and their geodynamic environments. Lithos 46, 605–626.

Beard, J., Lofgren, G., 1991. Dehydration melting and water-saturated melting of basaltic and andesitic greenstones and amphibolites at 1, 3, and 6. 9 kb. J. Petrol. 32, 365–401.

Blichert-Toft, J., Albarede, F., 1997. The Lu-Hf geochemistry of chondrites and the evolution of the mantle-crust system. Earth Planet. Sci. Lett. 148, 243–258.

Bouvier, A., Vervoort, J.D., Patchett, P.J., 2008. The Lu-Hf and Sm-Nd isotopic composition of CHUR: constraints from unequilibrated chondrites and implications for the bulk composition of terrestrial planets. Earth Planet. Sci. Lett. 273, 48–57.

Cai, Y.F., Wang, Y.J., Cawood, P.A., Fan, W.M., Liu, H.C., Xing, X.W., Zhang, Y.Z., 2014. Neoproterozoic subduction along the Ailaoshan zone, South China: geochronological and geochemical evidence from amphibolite. Precambr. Res. 245, 13–28.

Cai, Y.F., Wang, Y.J., Cawood, P.A., Zhang, Y.Z., Zhang, A.M., 2015. Neoproterozoic crustal growth of the Southern Yangtze Block: geochemical and zircon U-Pb geochronological and Lu-Hf isotopic evidence of Neoproterozoic diorit from the Ailaoshan zone. Precambr. Res. 266, 137–149.

Castro, A., Moreno-Ventas, I., de la Rosa, J.D., 1991. H-type (hybrid) granitoids: a proposed revision of the granite-type classification and nomenclature. Earth-Sci. Rev. 31, 237–253.

Chappell, B.W., White, A.J.R., Wyborn, D., 1987. The importance of residual source material (restite) in granite petrogenesis. J. Petrol. 28, 1111–1138.

Chappell, B.W., Bryant, C.J., Wyborn, D., 2012. Peraluminous I-type granites. Lithos 153, 142–153.

Chen, F.K., Siebel, W., Satir, M., Terzioglu, M., Saka, K., 2002. Geochronology of the Karadere basement (NW Turkey) and implications for the geological evolution of the Istanbul zone. Int. J. Earth Sci. 91, 469–481.

Chen, Q., Sun, M., Long, X.P., Yuan, C., 2015. Petrogenesis of Neoproterozoic adakitic tonalites and high-K granites in the eastern Songpan-Ganze Fold Belt and implications for the tectonic evolution of the western Yangtze Block. Precambr. Res. 270, 181–203.

Chung, S.L., Lee, T.Y., Lo, C.H., Wang, P.L., Chung, S.L., Yem, N.T., Hoa, T.T., Genyao, W., 1997. Intraplate extension prior to continental extrusion along the Ailao Shan-Red River shear zone. Geology 25, 311–314.

Collins, W.J., Richards, S.W., 2008. Geodynamic significance of S-type granites in circum-Pacific orogens. Geology 36, 559–562.

Ewart, A., Hawkesworth, C.J., 1987. The Pleistocene-Recent Tonga-Kermadec arc lavas: interpretation of new isotopic and rare earth data in terms of a depleted mantle source model. J. Petrol. 28, 495–530.

Faure, M., Lepvrier, C., Nguyen, V.V., Vu, T.V., Lin, W., Chen, Z.C., 2014. The South China block-Indochina collision: where, when, and how? J. Asian Earth Sci. 79, 260–274.

Foley, S.F., Jackson, S.E., Fryer, B.J., Greenough, J.D., Jenner, G.A., 1996. Trace element partition coefficients for clinopyroxene and phlogopite in an alkaline lamprophyre from Newfoundland by LAM-ICP-MS. Geochim. Cosmochim. Acta 60, 629–638.

Goolaerts, A., Mattielli, N., de Jong, J., Weis, D., Scoates, J.S., 2004. Hf and Lu isotopic reference values for the zircon standard 91500 by MC-ICP-MS. Chem. Geol. 206, 1–9.

Green, T.H., 1994. Experimental Studies of Trace-Element Partitioning Applicable to Igneous Petrogenesis - Sedona 16 Years Later. Chem. Geol. 117, 1–36.

Griffin, W.L., Pearson, N.J., Belousova, E., Jackson, S.E., van Achterbergh, E., O'Reilly, S.Y., Shee, S.R., 2000. The Hf isotope composition of cratonic mantle: LAM-MC-ICPMS analysis of zircon megacrysts in kimberlites. Geochim. Cosmochim. Acta 64, 133–147.

Griffin, W.L., Pearson, N.J., Belousova, E.A., Saeed, A., 2006. Comment: Hf-isotope heterogeneity in zircon 91500. Chem. Geol. 233, 358–363.

Grove, T.L., Gerlach, D.C., Sando, T.W., 1982. Origin of calc-alkaline series lavas at Medicine Lake Volcano by fractionation, assimilation and mixing. Contrib. Miner. Petrol. 80, 160–182.

Hoskin, P.W.O., Schaltegger, U., 2003. The composition of zircon and igneous and metamorphic petrogenesis. Rev. Mineral. Geochem. 53, 27–55.

Huang, X.L., Xu, Y.G., Li, X.H., Li, W.X., Lan, J.B., Zhang, H.H., Liu, Y.S., Wang, Y.B., Li, H.Y., Luo, Z.Y., Yang, Q.J., 2008. Petrogenesis and tectonic implications of Neoproterozoic, highly fractionated A-type granites from Mianning, South China. Precambr. Res. 165, 190–204.

Huang, X.L., Xu, Y.G., Lan, J.B., Yang, Q.J., Luo, Z.Y., 2009. Neoproterozoic adakitic rocks from Mopanshan in the western Yangtze Craton: partial melts of a thickened lower crust. Lithos 112, 367–381.

Jackson, S.E., Pearson, N.J., Griffin, W.L., Belousova, E.A., 2004. The application of laser ablation-inductively coupled plasma-mass spectrometry to in situ U-Pb zircon geochronology. Chem. Geol. 211, 47–69.

Jahn, B.M., Griffin, W.L., Windley, B.F., 2000. Continental growth in the Phanerozoic: evidence from Central Asian. Tectonophysics 328, vii–x.

Karsli, O., Dokuz, A., Uysal, I., Aydin, F., Chen, B., Kandemir, R., Wijbrans, J., 2010. Relative contributions of crust and mantle to generation of Campanian high-K calc-alkaline I-type granitoids in a subduction setting, with special reference to the Harsit Pluton, Eastern Turkey. Contrib. Miner. Petrol. 160, 467–487.

Kemp, A.I.S., Hawkesworth, C.J., Foster, G.L., Paterson, B.A., Woodhead, J.D., Hergt, J.M., Gray, C.M., Whitehouse, M.J., 2007. Magmatic and crustal differentiation history of granitic rocks from Hf–O isotopes in zircon. Science 315, 980–983.

Kemp, A.I.S., Hawkesworth, C.J., Collins, W.J., Gray, C.M., Blevin, P.L., Eimf, 2009. Isotopic evidence for rapid continental growth in an extensional accretionary orogen: the Tasmanides, eastern Australia. Earth Planet. Sci. Lett. 284, 455–466.

Lan, C.Y., Chung, S.L., Shen, J.J., Lo, C.H., Wang, P.L., Hoa, Tran.Trong., Thanh, Hoang. Huu., Mertzman, S.A., 2000. Geochemical and Sr–Nd isotopic characteristics of granitic rocks from northern Vietnam. J. Asian Earth Sci. 18, 267–280.

Lan, C.Y., Chung, S.L., Lo, C.H., Lee, T.Y., Wang, P.L., Li, H., Toan, D.V., 2001. First evidence for Archean continental crust in northern Vietnam and its implications for crustal and tectonic evolution in Southeast Asia. Geology 29, 219–222.

Leloup, P.H., Lacassin, R., Tapponnier, P., Schärer, U., Zhong, D., Liu, X., Zhang, L., Ji, S., Trinh, P., 1995. The Ailaoshan-Red River shear zone (Yunnan, China), Tertiary transform boundary of Indochina. Tectonophysics 252, 3–84.

Lepvrier, C., Maluski, H., Nguyen, V.V., Roques, D., Axente, V., Rangin, C., 1997. Indosinian NW-trending shear zones within the Truong Son belt (Vietnam) ^{40}Ar-^{39}Ar Triasic ages and Cretaceous to Cenozoic overprints. Tectonophysics 283, 105–127.

Lepvrier, C., Maluski, H., Tich, V.V., Leyreloup, A., Thi, P.T., Vuong, N.V., 2004. The Early Triassic Indosinian orogeny in Vietnam (Truong Son Belt and Kontum Massif): implications for the geodynamic evolution of Indochina. Tectonophysics 393, 87–118.

Li, X.H., Li, W.X., Li, Q.L., Wang, X.C., Liu, Y., Yang, Y.H., 2010. Petrogenesis and tectonic significance of the ~850 Ma Gangbian alkaline complex in South China: evidence from in-situ zircon U-Pb and Hf-O isotopes and whole-rock geochemistry. Lithos 114, 1–15.

Li, X.H., Tang, G.Q., Gong, B., Yang, Y.H., Hou, K.J., Hu, Z.C., Li, Q.L., Liu, Y., Li, W.X., 2013. Qinghu zircon: a working reference for microbeam analysis of U-Pb age and Hf and O isotopes. Chin. Sci. Bull. 58, 4647–4654.

Lin, T.H., Chung, S.L., Chiu, H.Y., Wu, F.Y., Yeh, M.W., Searle, M.P., Iizuka, Y., 2012. Zircon U-Pb and Hf isotope constraints from the Ailao Shan-Red River shear zone on the tectonic and crustal evolution of southwestern China. Chem. Geol. 291, 23–37.

Liu, J.L., Wang, A.J., Cao, S.Y., Zou, Y.X., Tang, Y., Chen, Y., 2008a. Geochronology and tectonic implication of migmatites from Diancangshan, western Yunnan, China. Acta Petrol. Sin. 24, 413–420 (in Chinese with English abstract).

Liu, Y.S., Hu, Z.C., Gao, S., Günther, D., Xu, J., Gao, C.G., Chen, H.H., 2008b. In situ analysis of major and trace elements of anhydrous minerals by LA-ICP-MS without applying an internal standard. Chem. Geol. 257, 34–43.

Liu, H.C., Wang, Y.J., Cawood, P.A., Fan, W.M., Cai, Y.F., Xing, X.W., 2015. Record of Tethyan ocean closure and Indosinian collision along the Ailaoshan suture zone (SW China). Gondwana Res. 27, 1292–1306.

Lugmair, G.W., Harti, K., 1978. Lunar initial $^{143}Nd/^{144}Nd$: differential evolution of the lunar crust and mantle. Earth Planet. Sci. Lett. 39, 349–357.

Mann, A.C., 1983. Trace element geochemistry of high alumina basalt-andesite-dacite-rhyodacite lavas of the main volcanic series of Santorini volcano, Greece. Contrib. Miner. Petrol. 84, 43–57.

Mclean, R.N., 2001. The Sin Quyen iron oxide-copper-gold-rare earth oxide mineralization of North Vietnam. In: Porter, T.M. (Ed.), Hydrothermal Iron Oxide Copper–Gold & Related Deposits: A Global Perspective, vol. 2. PGC Publishing, Adelaide, pp. 293–301.

Metcalfe, I., 2002. Permian tectonic framework and palaeogeography of SE Asia. J. Asian Earth Sci. 20, 551–566.

Metcalfe, I., 2006. Palaeozoic and Mesozoic tectonic evolution and palaeogeography of East Asian crustal fragments: the Korean Peninsula in context. Gondwana Res. 9, 24–46.

Metcalfe, I., 2012. Changsinggian (Late Permian) conodonts from Son La, northwest Vietnam and their stratigraphic and tectonic implications. J. Asian Earth Sci. 50, 141–149.

Middlemost, E.A.K., 1994. Naming materials in the magma/igneous rock system. Earth-Sci. Rev. 74, 193–227.

Nam, T.N., 2001. The emplacement age of Ca Vinh complex and Xom Giau complex: the first reliable evidence from analytical results SHRIMP U-Pb zircon (in Vietnamese). Geol. Mag. A262, 1–11.

Pearce, J.A., Harris, N.B.W., Tindle, A.G., 1984. Trace element discrimination diagrams for the tectonic interpretation of granitic rocks. J. Petrol. 25, 956–983.

Petford, N., Gallagher, K., 2001. Partial melting of mafic (amphibolitic) lower crust by periodic influx of basaltic magma. Earth Planet. Sci. Lett. 193, 483–499.

Pham, T.H., Chen, F.K., Wang, W., Nguyen, T.B.T., Bui, M.T., Nguyen, Q.L., 2009. Zircon U-Pb ages and Hf isotopic composition of the Posen granite in northwest Vietnam. Acta Petrol. Sin. 25, 3141–3152.

Pham, T.H., Chen, F.K., Zhu, X.Y., Wang, F., 2010. Zircon ages of Paragneisses from the Sinh Quyen Formation in Northwestern Vietnam and their geological significances. Earth Sci. J. China Univ. Geosci. 35, 201–210 (in Chinese with English abstract).

Pham, T.H., Chen, F., Me, L.T., Thuy, N.T.B., Siebel, W., Lan, T.G., 2012. Zircon U-Pb ages and Hf isotopic compositions from the Sin Quyen Formation: the Precambrian crustal evolution of northwest Vietnam. Int. Geol. Rev. 54. 1548-156.

Polyakov, G.V., Balykin, P.A., Tran, T.H., Ngo, T.P., Hoang, H.T., Tran, Q.H., Ponomarchuk, V.A., Lebedev, Y., Kireev, A.D., 1998. Evolution of the Mesozoic-Cenozoic magmatism in the Song Da rift and its contouring structures (northwestern Vietnam). Sov. Geol. Geophys. 39, 695–706 (in Russian).

Qi, L., Hu, J., Grégoire, D.C., 2000. Determination of trace elements in granites by inductively coupled plasma mass spectrometry. Talanta 51, 507–513.

Qi, X.X., Zeng, L.S., Zhu, L.H., Hu, Z.C., Hou, K.J., 2012. Zircon U-Pb and Lu-Hf isotopic systematics of the Daping plutonic rocks: implications for the Neoproterozoic tectonic evolution of the northeastern margin of the Indochina block, Southwest China. Gondwana Res. 21, 180–193.

Qi, X.X., Santosh, M., Zhu, L.H., Zhao, Y.H., Hu, Z.C., Zhang, C., Ji, F.B., 2014. Mid-Neoproterozoic arc magmatism in the northeastern margin of the Indochina block, SW China: geochronological and petrogenetic constraints and implications for Gondwana assembly. Precambr. Res. 245, 207–224.

Roberts, M., Clemens, J.D., 1993. Origin of high-potassium, calc-alkaline, I-type granitoids. Geology 21, 825–828.

Roger, F., Leloup, P.H., Jolivet, M., Lacassin, R., Tranh, P.T., Brunel, M., Seward, D., 2000. Long and complex thermal history of the Song Chay metamorphic dome (Northern Vietnam) by multi-system geochronology. Tectonophysics 321, 449–466.

Sisson, T., Ratajeski, K., Hankins, W., Glazner, A., 2005. Voluminous granitic magmas from common basaltic sources. Contrib. Miner. Petrol. 148, 635–661.

Söderlund, U., Patchett, P.J., Vervoort, J.D., Isachsen, C.E., 2004. The ^{176}Lu decay constant determined by Lu–Hf and U-Pb isotope systematics of Precambrian mafic intrusions. Earth Planet. Sci. Lett. 219, 311–324.

Sun, S.S., McDonough, W.F., 1989. Chemical and isotope systematics of oceanic basalts: implications for mantle composition and processes. In: Saunders, A.D. (Ed.), Magmatism in Ocean Basins. Geological Society Special Publication 42, London, pp. 313–345.

Sun, W.H., Zhou, M.F., Gao, J.F., Yang, Y.H., Zhao, X.F., Zhao, J.H., 2009. Detrital zircon U-Pb geochronological and Lu-Hf isotopic constraints on the Precambrian magmatic and crustal evolution of the western Yangtze Block, SW China. Precambr. Res. 172, 99–126.

Tapponnier, P., Lacassin, R., Leloup, P.H., Scharer, U., Zhong, D., Wu, H.H., Liu, X., Ji, S., Zhnag, L., Zhong, J., 1990. The Ailao Shan-Red River metamorphic belt: tertiary left-lateral shear between Sundaland and South China. Nature 343, 431–437.

Tran, T.V., Pang, K.W., Chung, S.L., Lin, H.M., Tran, T.H., Tran, T.A., Yang, H.J., 2011. The Song Da magmatic suite revisited: a petrologic, geochemical and Sr–Nd isotopic study on picrites, flood basalts and silicic volcanic rocks. J. Asian Earth Sci. 42, 1341–1355.

Tran, T.H., Lan, C.Y., Usuki, T., Shellnutt, J.G., Pham, T.D., Tran, T.A., Pham, N.C., Ngo, T.P., Izokh, A.E., Borisenko, A.S., 2015. Petrogenesis of Late Permian silicic rocks of Tu Le basin and Phan Si Pan uplift (NW Vietnam) and their association with the Emeishan large igneous province. J. Asian Earth Sci. 109, 1–19.

Trotter, J.A., Williams, I.S., Barnes, C.R., Lécuyer, C., Nicoll, R.S., 2008. Did cooling oceans trigger ordovician biodiversification? Evidence from conodont thermometry. Science 321, 550–554.

Usuki, T., Lan, C.Y., Wang, K.L., Chiu, H.Y., 2013. Linking the Indochina block and Gondwana during the Early Paleozoic: evidence from U-Pb ages and Hf isotopes of detrital zircons. Tectonophysics 586, 145–159.

Usuki, T., Lan, C.Y., Tran, T.H., Phan, T.D., Wang, K.L., Shellnutt, G.J., Chung, S.L., 2015. Zircon U-Pb ages and Hf isotopic compositions of alkaline silicic magmatic rocks in the Phan Si Pan-Tu Le region, northern Vietnam: identification of a displaced western extension of the Emeishan Large Igneous Province. J. Asian Earth Sci. 97, 102–124.

Valley, J.W., Lackey, J.S., Cavosie, A.J., Clechenko, C.C., Spicuzza, M.J., Basei, M.A.S., Bindeman, I.N., Ferreira, V.P., Sial, A.N., King, E.M., Peck, W.H., Sinha, A.K., Wei, C. S., 2005. 4.4 billion years of crustal maturation: oxygen isotopes in magmatic zircon. Contrib. Minera. Petrol. 150, 561–580.

Wang, X.L., Zhou, J.C., Qiu, J.S., Zhang, W.L., Liu, X.M., Zhang, G.L., 2006. LA-ICP-MS U-Pb zircon geochronology of the Neoproterozoic igneous rocks from Northern Guangxi, South China: implications for petrogenesis and tectonic evolution. Precambr. Res. 145, 111–130.

Wang, C.Y., Zhou, M.F., Qi, L., 2007a. Permian flood basalts and mafic intrusions in the Jinping (SW China)-Song Da (northern Vietnam) district: mantle sources, crustal contamination and sulfide segregation. Chem. Geol. 243, 317–343.

Wang, X.C., Li, X.H., Li, W.X., Li, Z.X., 2007b. Ca. 825 Ma komatiitic basalts in South China: first evidence for >1500 C mantle melts by a Rodinian mantle plume. Geology 35, 1103–1106.

Wang, P.L., Lo, C.H., Lan, C.Y., Chung, S.L., Lee, T.Y., Tran, N.N., Sano, Y., 2011. Thermochronology of the PoSen complex, northern Vietnam: implications for tectonic evolution in SE Asia. J. Asian Earth Sci. 40, 1044–1055.

Wang, X.L., Zhou, J.C., Wan, Y.S., Kitajima, K., Wang, D., Bonamici, C., Qiu, J.S., Sun, T., 2013. Magmatic evolution and crustal recycling for Neoproterozoic strongly peraluminous granitoids from southern China: Hf and O isotopes in zircon. Earth Planet. Sci. Lett. 366, 71–82.

Wang, W., Cawood, P.A., Zhou, M.F., Zhao, J.H., 2016. Paleoproterozoic magmatic and metamorphic events link Yangtze to northwest Laurentia in the Nuna supercontinent. Earth Planet. Sci. Lett. 433, 269–279.

Wiedenbeck, M., Alle, P., Corfu, F., Griffin, W.L., Meier, M., Oberli, F., Vonquadt, A., Roddick, J.C., Speigel, W., 1995. Three natural zircon standards for U-Th-Pb, Lu-Hf, trace-element and REE analyses. Geostand. Newslett. 19 (1), 1–23.

Wolf, M., Wyllie, P., 1994. Dehydration-melting of amphibolite at 10 kbar: the effects of temperature and time. Contrib. Miner. Petrol. 115, 369–383.

Wu, F.Y., Yang, Y.H., Xie, L.W., Yang, J.H., Xu, P., 2006. Hf isotopic compositions of the standard zircons in U-Pb geochronology. Chem. Geol. 234, 105–126.

Yue, J.P., Sun, X.M., Pham, H.T., Wang, P.J., Tien, D.L., Lang, Y.Q., Du, J.Y., 2013. Pre-Cenozoic tectonic attribution and setting of the Dong Da zone, Vietnam. Geotec. Metall. 37 (4), 561–570 (in Chinese with English abstract).

Yumul Jr., G.P., Zhou, M.F., Wang, C.Y., Zhao, T.P., Dimalanta, C.B., 2008. Geology and geochemistry of the Shuanggou ophiolite (Ailao Shan ophiolitic belt), Yunnan Province, SW China: evidence for a slow-spreading oceanic basin origin. J. Asian Earth Sci. 32, 385–395.

Zelazniewicz, A., Tran, T.H., Larionov, A.N., 2013. The significance of geological and zircon age data derived from the wall rocks of the Ailao Shan-Red River Shear Zone, NW Vietnam. J. Geodyn. 69, 122–139.

Zhang, Y.Z., Wang, Y.J., 2016. Early Neoproterozoic (~840 Ma) arc magmatism: geochronological and geochemical constraints on the metabasites in the Central Jiangnan Orogen. Precambr. Res. 275, 1–17.

Zhang, Y.Z., Wang, Y.J., Fan, W.M., Zhang, A.M., Ma, L.Y., 2012. Geochronological and geochemical constraints on the metasomatised source for the Neoproterozoic (~825 Ma) high-Mg volcanic rocks from the Cangshuipu area (Hunan Province) along the Jiangnan domain and their tectonic implications. Precambr. Res. 220–221, 139–157.

Zhao, G.C., Cawood, P.A., 2012. Precambrian geology of China. Precambr. Res. 222, 13–54.

Zhao, J.H., Zhou, M.F., 2008. Neoproterozoic adakitic suite at the northwestern margin of the Yangtze block, China: evidence for partial melting of thickened lower crust and secular crustal evolution. Lithos 104, 231–248.

Zhao, X.F., Zhou, M.F., Li, J.W., Wu, F.Y., 2008. Association of Neoproterozoic A- and I-type granites in South China: implications for generation of A-type granites in a subduction-related environment. Chem. Geol. 257, 1–15.

Zhao, J.H., Zhou, M.F., Yan, D.P., Zheng, J.P., Li, J.W., 2011. Reappraisal of the ages of Neoproterozoic strata in South China: no connection with the Grenvillian orogeny. Geology 39, 299–302.

Zheng, Y.F., Zhang, S.B., Zhao, Z.F., Wu, Y.B., Li, X.H., Li, Z.X., Wu, F.Y., 2007. Contrasting zircon Hf and O isotopes in the two episodes of Neoproterozoic granitoids in South China: implications for growth and reworking of continental crust. Lithos 96, 127–150.

Zheng, Y.F., Wu, R.X., Wu, Y.B., Zhang, S.B., Yuan, H.L., Wu, F.Y., 2008. Rift melting of juvenile arc-derived crust: geochemical evidence from Neoproterozoic volcanic and granitic rocks in the Jiangnan Orogen, South China. Precambr. Res. 163, 351–383.

Zhou, M.F., Yan, D.P., Kennedy, A.K., Li, Y., Ding, J., 2002. SHRIMP U-Pb zircon geochronological and geochemical evidence for Neoproterozoic arc-magmatism along the western margin of the Yangtze Block, South China. Earth Planet. Sci. Lett. 196, 51–67.

Zhou, X.M., Sun, T., Shen, W.Z., Shu, L.S., Niu, Y.L., 2006. Petrogenesis of Mesozoic granitoids and volcanic rocks in South China: a response to tectonic evolution. Episodes 29, 26–33.

Zhu, W.G., Zhong, H., Li, Z.X., Bai, Z.J., Yang, Y.J., 2016. SIMS zircon U-Pb ages, geochemistry and Nd–Hf isotopes of ca.1.0 Ga mafic dykes and volcanic rocks in the Huili area, SW China: origin and tectonic significance. Precambr. Res. 273, 67–89.